Saito *et al. Earth, Planets and Space* (2018) 70:197
https://doi.org/10.1186/s40623-018-0970-x

Earth, Planets and Space

FULL PAPER

Open Access

Petrological characteristics and volatile content of magma of the 1979, 1989, and 2014 eruptions of Nakadake, Aso volcano, Japan

Genji Saito*, Osamu Ishizuka, Yoshihiro Ishizuka, Hideo Hoshizumi and Isoji Miyagi

Abstract

Petrological observations and chemical analyses of melt inclusions in scoria were used to investigate the magma ascent and eruption processes of the 1979, 1989, and 2014 eruptions of Nakadake, Aso volcano, Japan. Major elements and sulfur contents of the melt inclusions were determined using an electron probe microanalyzer, and their water and CO_2 contents were determined using secondary ion mass spectrometry. Five scoria specimens from the 2014 eruptions had an andesite composition identical to the scoria from the 1979 and 1989 eruptions. Thermometry using the chemical composition of the groundmass and the rims of the phenocrysts indicated that the temperature of the 2014 magma was 1042–1092 °C. Melt inclusions in plagioclases, clinopyroxenes, and olivines in the 2014 scoria had an andesite composition similar to that of the groundmass. The volatile content of the melt inclusions was 0.6–0.8 wt% H_2O, 0.003–0.017 wt% CO_2, and 0.008–0.036 wt% S. The variation in CO_2 and S content of the melt inclusions was not correlated with the K_2O content, suggesting that the magma degassed as pressure decreased. Melt inclusions in plagioclases, clinopyroxenes, and olivines from the 1979 and 1989 scoria had similar major elements and volatile content to the 2014 eruption specimens. The similarity in chemical composition of both the whole-rock and melt inclusions among all samples suggests that the magmas of these eruptions were derived from the same magma chamber. The gas saturation pressure estimated from the H_2O and CO_2 contents of the 1979, 1989, and 2014 scoria ranged from 18 to 118 MPa, corresponding to depths of 1–4 km. Comparison of this depth with geophysical observations suggests that the inclusion entrapments occurred in the upper part of the magma chamber and/or a conduit. By combining the melt inclusion analysis with volcanic gas observations, we estimated the bulk volatile content of the magma. Based on the bulk sulfur content of the magma and the SO_2 flux between January 2014 and December 2017, the amount of degassed magma over that period was estimated to be the equivalent of 1–3 km^3 of dense rock. The estimated volume was more than 600 times larger than that of products erupted during the same period. This suggests that magma degassing occurred at several depths in the magma chamber due to magma convection in a conduit.

Keywords: Aso volcano, Nakadake, Magma, Eruption, Magma ascent, Degassing, Melt inclusion, Volatile, Magma plumbing system

*Correspondence: saito-g@aist.go.jp
Geological Survey of Japan, Advanced Industrial Science and Technology, Central 7, Higashi 1-1-1, Tsukuba, Ibaraki 305-8567, Japan

Introduction

The volatile content of magma is an important controlling factor in magma ascent and eruption processes. Melt inclusion analysis is a powerful method for estimating the volatile content of melt in magma before eruption (e.g., Anderson 1973; Anderson et al. 1989; Johnson et al. 1994; Lowenstern 2003; Metrich and Wallace 2008). Moreover, by combining the melt inclusion analysis with geophysical and geochemical observations, we can estimate the depth of the magma and the degassed magma volume (e.g., Saito et al. 2001, 2005; Saito 2005).

Nakadake, Aso volcano, is one of the most active volcanoes in Japan. Since the 1990s, various geophysical observations have been used to investigate the subsurface structure and plumbing system of the magma, including gravimetric observations (Komazawa 1995), seismic observations (Yamamoto et al. 1999; Sudo and Kong 2001; Tsutsui and Sudo 2004; Abe et al. 2010), and magnetotelluric surveys (Kanda et al. 2008; Hata et al. 2016). These surveys suggested the existence of a magma chamber at a depth of less than 20 km. In addition, geological observations were carried out to estimate the volume of the tephra created by recent eruptions (e.g., Kyoto Univ 1980; Ono and Watanabe 1985; Kumamoto Univ 2015a, b; Kumamoto Univ et al. 2016). Geochemical observations of volcanic gas were also conducted to estimate the flux and chemical composition of the emitted gas (Geological Survey of Japan 2015a; Japan Meteorological Agency 2018b; Shinohara et al. 2018). Together, these observations allowed the advancement of our understanding of the magma ascent and eruption processes.

In this study, we carried out petrological observations and chemical analyses of melt inclusions of the scoria from recent eruptions at Nakadake in 1979, 1989, and 2014. Our objectives were (1) to determine the petrologic characteristics of the magmas of the eruptions and their changes over time, (2) to investigate the volatile content of the magmas, the depth of the magma chamber, and the amount of degassed magma, and (3) to combine these parameters with geological and geophysical observations to model the magma ascent processes at Nakadake, Aso volcano.

Overview of Nakadake, Aso volcano and the 1979, 1989, and 2014 eruptions

Aso volcano is located in central Kyushu, western Japan (Fig. 1). This volcano became active about 300 ka, and four caldera-forming eruptions occurred by 90 ka (e.g., Ono and Watanabe 1985; Machida and Arai 2003). The post-caldera eruptions started soon after the caldera-forming eruptions, and the total volume of tephra and edifices of the post-caldera central cones was about 130 km^3 dense rock equivalent (DRE) (Miyabuchi et al. 2004; Miyabuchi 2009, 2011). Volcanic activities of Nakadake, one of the post-caldera volcanoes, started around 22–21 ka (Miyabuchi 2009)

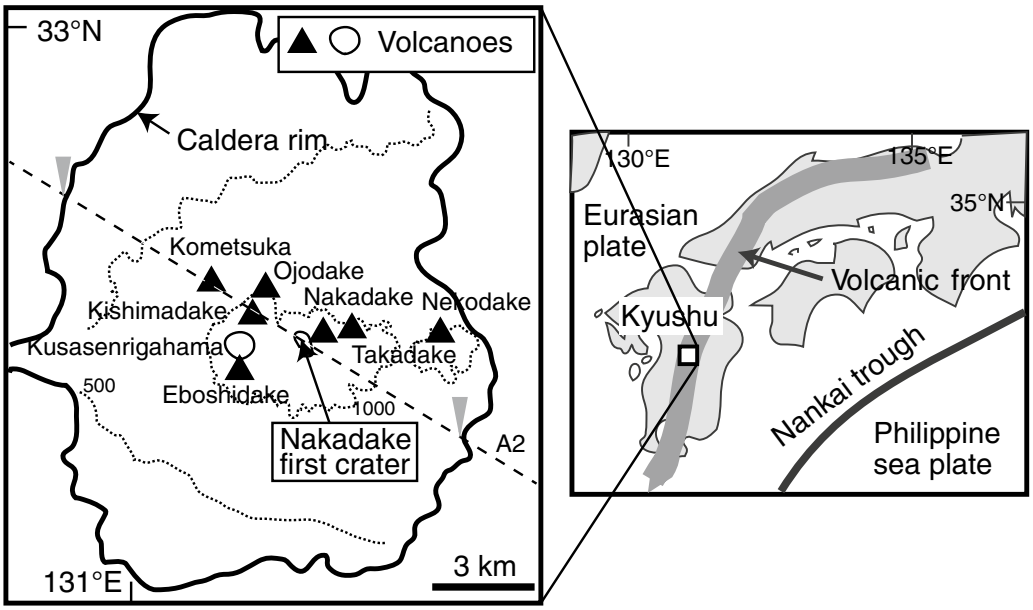

Fig. 1 Maps of the Nakadake and Nakadake first crater, Aso volcano. The right figure shows the location of the Aso volcano in southwest Japan, and the left figure shows the locations of representative post-caldera volcanoes (< 90 ka), except for Nakadake, which formed 150 ka. The dashed black line labeled A2 in the left figure indicates the profile used by Hata et al. (2016) to estimate the cross section of three-dimensional electrical resistivity

and continued through the present (JMA 2013). The recent activity in 1976–1979, 1988–1990, and 2014–2016 at Nakadake has been characterized by a cycle of drying-up of the crater lake water followed by mud eruptions, then phreato- and phreato-magmatic eruptions, and finally Strombolian eruptions (e.g., Asosan Weather Station 1980; Kyoto Univ 1980; JMA 1990; Ono et al. 1995; Ikebe et al. 2008). The emission rate of SO_2 from the crater also increased as the activity increased: less than 2 kg s^{-1} (160 t d^{-1}) in 1976–1977 to 12 kg s^{-1} (1000 t d^{-1}) in September 1979 and then 30 kg s^{-1} (2600 t d^{-1}) in November 1979 (Kyushu Univ 1980). The total tephra produced by the 1979 eruptions was about 9.5×10^9 kg (3.5×10^6 m^3 DRE; Kyushu Univ 1980; Ono and Watanabe 1985). Similarly, from 1988 to 1989, the SO_2 emission rate from the crater increased from less than 12 kg s^{-1} (1000 t d^{-1}) in 1988, prior to the eruptions, to 44 kg s^{-1} (3800 t d^{-1}) during the climactic period (October to November 1989) and then returned to less than 12 kg s^{-1} (1000 t d^{-1}) in 1990 (Kyushu Univ 1990). The most recent eruption series started with minor eruptions in January 2014 after an increase in earthquakes in 2013, followed by Strombolian eruptions on November 26–27, 2014 (JMA 2015), and more intermittent eruptions until October 2016 (JMA 2018a). The total tephra produced by the 2014 eruptions (November 25–29 and December 9–11) and the most recent large eruption, which occurred on October 8, 2016, was estimated to be about 0.2×10^9 kg (7×10^4 m^3 DRE; Kumamoto Univ 2015a, b) and $0.6–0.7 \times 10^9$ kg ($2–3 \times 10^5$ m^3 DRE; Kumamoto Univ et al. 2016), respectively. SO_2 emission rates exceeded 12 kg s^{-1} (1000 t d^{-1}) starting in January 2014, peaked at 174 kg s^{-1} (15,000 t d^{-1}) at the time of the explosive eruption on October 8, 2016, and continued until December 2017 (JMA 2018b). Geochemical observations of the volcanic gas composition by multi-GAS (Aiuppa et al. 2005; Shinohara 2013) on January 12, 2015, just after the November 25–26, 2014, eruption, showed two types of gas being emitted: One was associated with ash eruptions (type A; molar ratios $CO_2/H_2O = 0.04$, $CO_2/SO_2 = 1$ and $H_2O/SO_2 = 25$) and the other was fumarole, a gas emitted from the crater side wall (type B; $CO_2/H_2O = 0.2$, $CO_2/SO_2 = 10$ and $H_2O/SO_2 = 45$ in mol; GSJ 2015a). Apparent equilibrium temperatures (AETs) of the type A and B gases were calculated from H_2O, SO_2, H_2S, and H_2 contents in the gases, with an assumption of equilibrium among these gas components. The AETs were high (975 °C and 680 °C, GSJ 2015a), suggesting that the gases were magmatic in origin. The observed chemical composition of the gas emitted from 2010 to 2015 could be explained by a mixture of the type A and B gases (GSJ 2015a).

Analytical methods

The major-element composition of the five 2014 scoria specimens was determined (Table 1) using wavelength-dispersive X-ray fluorescence analysis (XRF; Togashi 1989). Petrological observation on scoria from the Strombolian eruption on June 6, 1979 (sample ID AS790616S, called "the 1979 scoria" in this paper), scoria from the eruption on November 24, 1989 (sample ID AS891124 called "the 1989 scoria" in this paper), and scoria from the eruption on November 26–27, 2014 (called "the 2014 scoria" in this paper), were carried out as follows. The specimens were mounted in epoxy resin, ground with sand paper, and then polished with diamond powder (1 μm). The mode compositions and porosities of the specimens were determined (Table 2) using backscattered electron (BSE) images obtained by scanning electron microscopy (SEM) of cross sections of the scoria. Chemical analyses of phenocrysts, melt inclusions, microlites (< 0.1 mm), glass in the groundmass, and the bulk composition of groundmass (called "groundmass bulk" in this paper) were conducted using an electron probe microanalyzer (EPMA; JEOL JXA-8900 at GSJ, AIST). The experimental conditions used for the analysis of minerals and groundmass bulk were identical to those reported by Saito et al. (2002) and Saito et al. (2001). The major-element contents and the minor S and Cl contents of melt inclusions and glass in the groundmass were determined with the EPMA using an accelerating voltage of 15 keV, a beam current of 12 nA, and a defocused 5-μm-diameter beam (Tables 3 and 4). The details of the experimental conditions for the EPMA analysis are described in Saito et al. (2010). Analytical errors on the S and Cl contents were ±0.007 wt% and ±0.004 wt%, respectively (Saito et al. 2010). We also estimated the H_2O content of the inclusions and the glass in the groundmass with the EPMA by assuming that the H_2O content was equal to the difference between 100% and the sum of all other measured oxide contents. The error of this method is ±1 wt% of the obtained measurements based on repeated analyses of standard glass samples.

We measured the H_2O and CO_2 contents of melt inclusions and glass in the groundmass of the 1979, 1989, and 2014 scoria by secondary ion mass spectrometry (SIMS) (Tables 3 and 4). Prior to the SIMS analyses, the mounted samples were polished with Al_2O_3 powder (1 μm). All mounted samples were coated with gold for the SIMS analyses. We used a Cameca IMS-1270 SIMS (installed at GSJ, AIST) to measure the H_2O and CO_2 contents of the melt inclusions. Cs^+ ions were used as the primary beam and negatively charged secondary ions of ^1H, ^{12}C, and ^{30}Si were collected (Hauri et al. 2002). The defocused Cs^+ primary beam was restricted to 25 μm in diameter by a circular aperture to obtain a homogeneous primary

Table 1 Whole-rock composition of scoria from the November 26–27, 2014, eruption (wt%). The composition of scoria from the 1979 and 1989 eruptions is also shown

Eruptions	1979			1989				November 26–27, 2014				
Sample ID	GK790616	GK791126	OW1985	ASO891006	ASO891010	ASO891012	ASO891014	1127 K-2	I141129S01	I141129S02	I141129S03	I141129S04
SiO_2	54.64	54.37	54.16	53.97	53.95	54.03	53.96	54.05	54.24	53.93	53.97	53.87
TiO_2	0.93	0.88	0.88	0.98	0.97	0.94	0.97	0.96	0.94	0.93	0.96	0.96
Al_2O_3	18.07	18.49	18.42	16.97	17.40	17.91	17.54	18.10	17.90	18.20	17.99	17.95
FeOt	8.23	8.31	8.34	8.86	8.74	8.40	8.53	8.45	8.54	8.33	8.59	8.55
MnO	0.15	0.15	0.15	0.16	0.15	0.15	0.15	0.16	0.17	0.16	0.16	0.17
MgO	3.69	3.47	3.48	3.99	3.84	3.48	3.63	3.76	3.95	3.70	3.92	3.77
CaO	8.76	8.77	8.74	8.56	8.50	8.62	8.54	8.59	8.86	8.72	8.75	8.67
Na_2O	3.03	2.95	3.38	3.03	3.13	3.07	3.19	3.08	3.01	3.05	3.03	3.00
K_2O	1.91	2.02	2.01	2.02	2.01	2.00	2.04	2.03	1.96	1.97	1.97	2.03
P_2O_5	0.26	0.29	0.29	0.30	0.30	0.29	0.30	0.29	0.28	0.28	0.28	0.28
Total	99.67	100.40	99.85	98.84	98.99	98.89	98.85	100.40	100.79	100.20	100.59	100.20

FeOt: Total FeO

Data on two 1979 scoria (GK790616 and GK791126) and four 1989 scoria are from GSJ and Kumamoto Univ (1990)

Data on OW1985 is scoria of November 1979 eruption from Ono and Watanabe (1985)

Samples I141129S01-04 were collected by GSJ and 1127 K-2 by JMA

Table 2 Mode composition of scoria from the November 26–27, 2014, eruption (vol%). Porosity of the scoria and volume fraction of glass in groundmass are also shown (vol%)

Sample ID	I141129S01	I141129S02	I141129S03
Phenocryst	37	35	39
Plagioclase	22	28	31
Olivine	2	2	2
Clinopyroxene	13	5	6
Fe–Ti oxide	< 1	0	< 1
Groundmass	63	65	61
Porosity	65	77	50
Glass in groundmass	90	65	3

Number of points: 2098 for I141129S01, 3459 for I141129S02, 4177 for I141129S03

beam of about 1 nA. Negative ions of ^{1}H, ^{12}C, and ^{30}Si were detected using a total impact energy of 20 kV. The analyzed area of the sample surface was limited to a central square measuring 10 × 10 μm to avoid the crater edge effect (Saito et al. 2010). A normal-incidence electron gun was used for charge compensation on the sample based on Kita et al. (2004). We made SIMS calibration lines for H_2O and CO_2 on each measurement day using the reference glasses. A more detailed description of the SIMS analyses is provided in Saito et al. (2010).

Results

Chemical compositions of the scoria

The five 2014 scoria specimens have identical andesite whole-rock composition (54 wt% SiO_2 and 2.0 wt% K_2O as recalculated to 100% on a water-free basis; Table 1; Fig. 2). In addition, the whole-rock compositions are identical to those of the 1979 and 1989 scoria (54–55 wt% SiO_2 and 1.9–2.0 wt% K_2O and 55 wt% SiO_2 and 2.0–2.1 wt% K_2O, respectively). The products of the 1929, 1933, 1958, and 1974 eruptions have slightly less evolved compositions and display greater variability than those of the 1979–2014 eruptions (53–54 wt% SiO_2 and 1.5–1.9 wt% K_2O; GSJ and Kumamoto Univ 1990; Fig. 2).

Three of the 2014 scoria specimens have a phenocryst content of 35–39 vol%, composed of 22–31 vol% plagioclase phenocrysts, 5–13 vol% clinopyroxene phenocrysts, and a small percentage by volume of olivine and FeTi oxide phenocrysts (Table 2). The groundmass of the 2014 scoria consists of 50–77 vol% of bubbles, with the remaining vol% made up of glass, plagioclases, clinopyroxenes, olivines, and FeTi oxides, with a large variation in glass content in the groundmass (3–90 vol%). Previous studies (Ono and Watanabe 1985; GSJ and Kumamoto Univ 1990) reported that the 1979 and 1989 scoria contained phenocrysts of plagioclase, clinopyroxene, olivine, and FeTi oxide. The 2014 scoria contain the same kinds of phenocrysts as in 1979 and 1989 scoria, consistent with the whole-rock composition of these specimens being identical.

The plagioclase phenocrysts of the three 2014 scoria specimens have cores of $An_{62–91}$ and rims of $An_{60–79}$ (Fig. 3). The plagioclase phenocrysts of the 1979 and 1989 scoria have cores of $An_{60–76}$ and rims of $An_{60–70}$, similar to the 2014 scoria, although the cores of the 2014 scoria have a larger An range (Fig. 3). Groundmass plagioclase cores of the 2014 scoria contain $An_{50–65}$, except a single groundmass plagioclase, which has a slightly lower An than the rim of the plagioclase phenocrysts. The cores and rims of the olivine phenocrysts in the 2014 scoria specimens fall within a narrow range of core $Fo_{65–68}$ and rim $Fo_{59–68}$. The cores and rims of the olivine phenocrysts in the 1979 scoria have chemical compositions similar to those of the 2014 scoria. The clinopyroxene phenocrysts of the 2014 scoria have cores of $Wo_{36–41}En_{43–47}Fs_{15–20}$ and rims of $Wo_{36–40}En_{42–46}Fs_{17–19}$. One clinopyroxene phenocryst has an orthopyroxene inclusion with a core chemical composition of $W_4En_{66}Fs_{30}$ (Additional file 1: Fig. S1). The cores and rims of the clinopyroxene phenocrysts in the 1979 and 1989 scoria have similar chemical compositions to those of the 2014 scoria. Similarity between the chemical compositions of the plagioclases, olivines, and clinopyroxenes among the 1979, 1989, and 2014 scoria indicates that they crystallized under the same physical and chemical magma conditions.

The groundmass bulk of the three 2014 scoria specimens has an andesitic composition: 59 wt% SiO_2 and 3.2–3.4 wt% K_2O (Table 4; Fig. 2). The groundmass glass in the two 2014 scoria specimens has a similar andesitic composition of 59 wt% SiO_2 and 3.4–3.7 wt% K_2O (Table 4; Fig. 2). The groundmass glass of the 1979 and 1989 scoria also has a similar composition of 59 wt% SiO_2 and 3.7 wt% K_2O and 58 wt% SiO_2 and 3.3–3.5 wt% K_2O, respectively (Table 4; Fig. 2). Furthermore, the 2003 ash particles have a similar composition of 58 wt% SiO_2 and 3.5 wt% K_2O (Table 4; Fig. 2; GSJ et al. 2004). The similarity in the chemical composition of groundmass glass of the 1979, 1989, and 2014 scoria and the 2003 ash particles is consistent with the hypothesis that these materials were derived from the same magma.

Melt inclusions

Melt inclusions in the 1979, 1989, and 2014 scoria are glassy and round to elliptical in shape and range in size from 0.01 to 0.2 mm (Fig. 4; Table 3). Melt inclusions in plagioclases, clinopyroxenes, and olivines in the 1979 scoria have an andesite composition of 57–62 wt% SiO_2 and 3.2–4.5 wt% K_2O (Fig. 2). Melt inclusions in

Table 3 Chemical composition of melt inclusions in the scoria from the 1979, 1989, and 2014 eruptions analyzed by EPMA and SIMS (wt%). Gas saturation pressure calculated from the H_2O and CO_2 content of the melt inclusions and temperature and pressure of the magma estimated with thermobarometers proposed by Putirka (2008) are also shown

	1979.6.16 scoria					
Sample ID	**AS790616S**	**AS790616S**	**AS790616S**	**AS790616S**	**AS790616S**	**AS790616S**
MI no.	**mts10120601-2-p6i2**	**mts10120608-2-p5i1**	**mts10120601-3-p2i1**	**mts10120601-3-p2i2**	**mts10120608-2-p3i1**	**mts10120608-2-p4i1**
Host phenocryst	**Pl(An66)**	**Pl(An63)**	**Cpx(Wo37En44Fs19 Mg#70)**	**Cpx(Wo38En43Fs18 Mg#70)**	**Cpx(Wo37En44Fs19 Mg#70)**	**Cpx(Wo38En43Fs19 Mg#69)**
Size of MI	**0.12 × 0.05 (mm)**	**0.10 × 0.04 (mm)**	**0.08 × 0.05 (mm)**	**0.10 × 0.10 (mm)**	**0.06 × 0.04 (mm)**	**0.07 × 0.06 (mm)**
SiO_2	54.39	59.57	56.01	55.81	56.22	58.35
TiO_2	1.49	1.14	1.41	1.30	1.36	1.35
Al_2O_3	14.03	14.27	13.68	13.47	14.19	13.41
FeOt	10.20	6.99	10.59	11.53	9.09	9.11
MnO	0.18	0.09	0.19	0.25	0.17	0.19
MgO	2.88	1.85	2.46	2.81	2.36	2.12
CaO	5.68	4.57	5.75	5.98	5.18	4.74
Na_2O	2.99	3.18	2.71	2.78	3.28	2.74
K_2O	3.26	4.21	3.25	3.08	3.79	4.28
P_2O_5	0.32	0.12	0.26	0.23	0.32	0.29
S	0.021	0.013	0.015	0.019	0.010	0.018
Cl	0.075	0.065	0.071	0.074	0.074	0.088
H_2O (SIMS/EPMA)[a]	0.3/1.3	1.2/1.0	0.6/0.9	0.6/0.5	0.9/1.0	1.3/0.8
CO_2 (SIMS)[b]	0.012	0.034	0.024	0.020	0.009	0.025
S(+6)/total S[c]	0.2	0.3	0.8	0.6	n.a.	0.6
log fO_2[d]	−9	−9	−8	−8	n.a.	−8
Fe(+2)/total Fe[e]	0.7	0.8	0.8	0.7	n.a.	0.7
NNO (log unit)[f]	−0.4	0.0	0.8	0.5	n.a.	0.5
Sat. Press. (MPa)[g]	61	118	102	98	51	113
Temperature (°C)[h]	1066	1046	1074	1073	1062	1059
Pressure (MPa) (cpx–liquid)[h]			440	410	390	560
K_D^i	0.17	0.13	0.22	0.23	0.25	0.24

Table 3 (continued)

	1979.6.16 scoria	1989.11.24 scoria				
Sample ID	**AS790616S**	**AS891124**	**AS891124**	**AS891124**	**AS891124**	**AS891124**
MI no.	**mts10120608-2-p1i1**	**mts10120601-4-p1i1**	**mts10120601-4-p3i1**	**mts10120608-4-p1i1**	**mts10120608-4-p3i1**	**mts10120608-4-p3i2**
Host phenocryst	**Ol(Fo65)**	**Cpx(Wo38En44Fs18 Mg#71)**	**Cpx(Wo37En43Fs20 Mg#68)**	**Cpx(Wo37En43Fs20 Mg#69)**	**Cpx(Wo39En43Fs19 Mg#70)**	**Cpx(Wo40En43Fs18 Mg#71)**
Size of MI	**0.20 x 0.10 (mm)**	**0.20 x 0.10 (mm)**	**0.10 x 0.06 (mm)**	**0.15 x 0.10 (mm)**	**0.10 x 0.10 (mm)**	**0.09 x 0.09 (mm)**
SiO_2	57.66	58.40	59.24	58.44	59.71	57.92
TiO_2	1.29	1.49	1.27	1.27	1.40	1.37
Al_2O_3	13.47	14.30	14.42	14.60	14.24	14.67
FeOt	9.78	9.92	8.09	8.97	7.99	9.57
MnO	0.17	0.18	0.14	0.16	0.18	0.24
MgO	2.51	1.99	1.93	1.99	1.91	1.65
CaO	5.22	5.17	5.15	4.95	5.74	4.79
Na_2O	2.87	2.96	2.90	2.91	2.49	3.21
K_2O	3.52	3.83	3.57	3.89	3.38	4.39
P_2O_5	0.29	0.36	0.27	0.29	0.28	0.23
S	0.018	0.016	0.015	0.012	0.015	0.019
Cl	0.087	0.090	0.070	0.086	0.081	0.080
H_2O (SIMS/EPMA)[a]	1.6/0.7	0.6/0.2	0.5/0.6	0.5/0.4	0.5/0.5	0.3/0.3
CO_2 (SIMS)[b]	0.007	0.009	0.004	0.007	0.006	0.003
S(+6)/total S[c]	0.5	0.1	0.7	0.0	0.1	0.1
log fO_2[d]	−9	−10	−8	−10	−9	−10
Fe(+2)/total Fe[e]	0.8	0.9	0.7	0.9	0.8	0.9
NNO (log unit)[f]	0.2	−0.9	0.7	−1.2	−0.5	−0.9
Sat. Press. (MPa)[g]	53	50	18	37	22	21
Temperature (°C)[h]	1034	1058	1071	1055	1068	1031
Pressure (MPa) (cpx–liquid)[h]		460	560	440	470	280
K^i_D	0.31	0.18	0.25	0.22	0.23	0.16

Table 3 (continued)

	2014.11.26–27 scoria				
Sample ID	**I141129S01**	**I141129S**	**I141129S**	**I141129S02**	**I141129S03**
MI no.	**mts16041403-2-p1i1**	**mts16041403-4-p1i1**	**mts16041403-4-p1i2**	**I141129S02-1-p4i1**	**I141129S03-1-p1i1**
Host phenocryst	**Pl(An60)**	**Pl(An65)**	**Pl(An65)**	**Pl(An76)**	**Pl(An63)**
Size of MI	**0.10 x 0.08 (mm)**	**0.10 x 0.04 (mm)**	**0.08 x 0.04 (mm)**	**0.05 x 0.02 (mm)**	**0.04 x 0.01 (mm)**
SiO_2	62.12	57.96	57.65	56.33	56.21
TiO_2	0.91	1.32	1.34	1.38	1.32
Al_2O_3	14.51	14.36	14.34	13.35	13.39
FeOt	7.53	9.47	9.80	9.30	9.09
MnO	0.14	0.14	0.16	0.18	0.21
MgO	1.96	2.99	2.66	2.71	2.75
CaO	4.30	5.92	5.58	5.53	5.03
Na_2O	3.10	3.02	3.27	2.60	2.65
K_2O	4.66	3.52	3.68	3.54	3.86
P_2O_5	0.31	0.64	0.62	0.31	0.23
S	0.008	0.015	0.014	0.018	0.029
Cl	0.055	0.087	0.075	0.075	0.071
H_2O (SIMS/EPMA)[a]	0.8/0.1	0.7/0.2	0.7/0.3	na/1.5	na/2.0
CO_2 (SIMS)[b]	0.002	0.008	0.017	na	na
S(+6)/total S[c]	0.1	0.4	0.1	na	na
log fO_2[d]	−9	−9	−9	na	na
Fe(+2)/total Fe[e]	0.8	0.8	0.8	na	na
NNO (log unit)[f]	−0.5	0.1	−0.4	na	na
Sat. Press. (MPa)[g]	27	41	80	na	na
Temperature (°C)[h]	1040	1081	1078	1059	1027
Pressure (MPa) (cpx–liquid)[h]					
K_D^i	0.14	0.17	0.15	0.11	0.18

Table 3 (continued)

	2014.11.26–27 scoria				
Sample ID	**I141129S**	**I141129S02**	**I141129S01**	**I141129S**	**I141129S02**
MI no.	**mts16041403-4-p2i1**	**I141129S02-1-p11i2**	**mts16041403-2-p2i1**	**mts16041403-3-p1i1**	**I141129S02-1-p12i1**
Host phenocryst	**Cpx(Wo38En43Fs19 Mg#69)**	**Cpx(Wo38En45Fs18 Mg#71)**	**Ol(Fo67)**	**Ol(Fo66)**	**Ol(Fo67)**
Size of MI	**0.10 x 0.05 (mm)**	**0.02 x 0.02 (mm)**	**0.08 x 0.07 (mm)**	**0.20 x 0.20 (mm)**	**0.02 x 0.02 (mm)**
SiO_2	58.21	54.89	57.93	58.11	56.34
TiO_2	1.21	1.45	1.38	1.20	1.34
Al_2O_3	14.55	14.35	14.51	14.37	14.13
FeOt	9.69	9.50	9.99	9.43	9.02
MnO	0.21	0.17	0.15	0.19	0.15
MgO	2.71	2.28	2.64	2.55	2.50
CaO	5.67	5.96	5.89	5.66	5.66
Na_2O	3.67	3.14	3.07	2.92	2.97
K_2O	3.05	3.25	3.43	3.64	3.45
P_2O_5	0.44	0.24	0.52	0.51	0.23
S	0.009	0.036	0.013	0.010	0.019
Cl	0.074	0.079	0.068	0.079	0.072
H_2O(SIMS/EPMA)[a]	0.6/0.1	na/1.5	0.7/0.1	0.7/0.6	na/1.0
CO_2 (SIMS)[b]	nd	na	0.003	0.004	na
S(+6)/total S[c]	na	na	0.4	0.7	na
log fO_2[d]	na	na	−9	−8	na
Fe(+2)/total Fe[e]	na	na	0.8	0.7	na
NNO (log unit)[f]	na	na	0.1	0.7	na
Sat. Press. (MPa)[g]	na	na	22	25	na

Table 3 (continued)

	2014.11.26–27 scoria				
Sample ID	**I141129S**	**I141129S02**	**I141129S01**	**I141129S**	**I141129S02**
MI no.	**mts16041403-4-p2i1**	**I141129S02-1-p11i2**	**mts16041403-2-p2i1**	**mts16041403-3-p1i1**	**I141129S02-1-p12i1**
Host phenocryst	**Cpx(Wo38En43Fs19 Mg#69)**	**Cpx(Wo38En45Fs18 Mg#71)**	**Ol(Fo67)**	**Ol(Fo66)**	**Ol(Fo67)**
Size of MI	**0.10 x 0.05 (mm)**	**0.02 x 0.02 (mm)**	**0.08 x 0.07 (mm)**	**0.20 x 0.20 (mm)**	**0.02 x 0.02 (mm)**
Temperature (°C)[h]	1071	1072	1046	1046	1042
Pressure (MPa) (cpx–liquid)[h]	420	460			
K_D^i	0.28	0.21	0.30	0.31	0.31

K_D of the melt inclusions in olivines = (X(ol-Fe)/X(ol-Mg))/(X(liq-FeO)/X(liq-MgO)). X(ol-Fe) and X(ol-Mg) are mol fractions of fayalite and forsterite in olivine, and X(liq-FeO) and X(liq-MgO) are cation fraction of Fe(+2) and Mg in the melt. The mol fraction ratio of Fe(+2) to total Fe in the melt was assumed to be 0.8. At equilibrium, this K_D is 0.299 ± 0.053 for P<2 GPa (Putirka 2008)

K_D of the clinopyroxene-hosted inclusions = − (X(cpx-Fe)/X(cpx-Mg))/(X(liq-FeO)/X(liq-MgO)). X(cpx-Fe) and X(cpx-Mg) are mol fractions of forsterite and enstatite in clinopyroxene, and X(liq-FeO) and X(liq-MgO) are cation fraction of Fe(+2) and Mg in the melt. The mol fraction ratio of Fe(+2) to total Fe in the melt was assumed to be 0.8. At equilibrium, this K_D is 0.28 ± 0.08 (Putirka 2008)

FeOt, total FeO; nd, not detected; na, not analyzed

[a] x/y: x, analyzed by SIMS, y, analyzed by EPMA. The analytical errors is ± 0.2 wt% for SIMS (Saito et al. 2010) and ± 1 wt% for EPMA

[b] The analytical error is ± 0.0028 wt% (Saito et al. 2010)

[c] Mol fractions of S(+6) in total S in the melt inclusions calculated from the S Kα radiation wavelength measured by EPMA, assuming that all S in the inclusions is composed of S(+6) and S(− 2)

[d] Calculated from the mol fraction of S(+6) in total S in the inclusions by Wallace and Carmichael (1994), assuming temperature of 1079 °C

[e] Calculated from the oxygen fugacity and chemical composition of the inclusions by Kilinc et al. (1983), assuming temperature of 1079 °C

[f] Estimates with 1079 °C

[g] Saturation pressures calculated from H_2O and CO_2 contents of the melt inclusions using the solubility model of Papale et al. (2006). An online version of the Papale's solubility model (http://melts.ofm-research.org/CORBA_CTserver/Papale/Papale.php) was used for these calculations. The mol ratio of Fe(+2) to total Fe in the melt and temperature was assumed to be 0.8 and 1079 °C, respectively

[h] Temperatures of the melt inclusions in plagioclases were estimated from chemical compositions of the melt and their host phenocrysts using plagioclase–liquid thermometer by Putirka (2008, Eq. (24a)). This thermometer yields a standard error of estimate (SEE) of 36 °C. Temperature of the melt inclusions in olivines was estimated from chemical compositions of the melt and their host phenocrysts using olivine–liquid thermometer by Putirka (2008, Eq. (22)). This thermometer yields SEE of 29 °C. Temperature and pressure of the melt inclusions in clinopyroxenes were estimated from chemical compositions of the melt and their host phenocrysts using clinopyroxene–liquid thermobarometers by Putirka (2008; Eqs. (31) and (33)). These thermobarometers yield SEE of 42 °C and 290 MPa. Saturation pressures and H_2O contents of the melt inclusions analyzed by SIMS were used for this calculationin. If the saturation pressures were not determined, pressure of 100 MPa was assumed. If the inclusions were not analyzed by SIMS, the H_2O contents analyzed by EPMA were used

[i] K_D of the melt inclusions in plagioclases = X(pl-Ab)X(liq-$AlO_{1.5}$)X(liq-CaO)/(X(pl-An)X(liq-$NaO_{0.5}$)X(liq-SiO_2)). X(pl-Ab) and X(pl-An) are mol fraction of albite and anorthite in plagioclase, and X(liq-$AlO_{1.5}$), X(liq-CaO), X(liq-$NaO_{0.5}$) and X(liq-SiO_2) are cation fractions of Al, Ca, Na and Si in the melt (Putirka 2008). At equilibrium, this K_D is 0.10 ± 0.05 for T < 1050 °C, and 0.27 ± 0.11 for T ≥ 1050 °C (Putirka 2008)

Table 4 Chemical composition of glass in groundmass and groundmass bulk in the scoria and the ash particles from the 1979, 1989, 2003, and 2014 eruptions (wt%)

Sample ID	1979.6.16 scoria		1989.10.15 scoria	1989.11.24 scoria	2003.7.10 ash particles[b]
	AS790616S	mts10120608−2−p1mg1	AS89101501	AS891124	
	Glass in groundmass	Glass in groundmass	Glass in groundmass	Glass in groundmass	Glass in groundmass
	Av ($n=30$, 1 s)		Av ($n=40$, 1 s)	Av ($n=20$, 1 s)	Av ($n=13$, 1 s)
SiO_2	59.19 (0.67)	53.70	58.16 (0.52)	58.00 (1.14)	58.09 (0.71)
TiO_2	1.42 (0.05)	1.23	1.37 (0.03)	1.34 (0.06)	1.38 (0.05)
Al_2O_3	14.10 (0.22)	14.87	14.35 (0.15)	14.49 (0.22)	14.40 (0.27)
FeOt	9.71 (0.29)	9.25	9.51 (0.20)	9.62 (0.33)	9.73 (0.27)
MnO	0.20 (0.02)	0.16	0.20 (0.03)	0.19 (0.02)	0.19 (0.03)
MgO	2.55 (0.10)	2.75	2.85 (0.10)	3.10 (0.25)	2.89 (0.18)
CaO	5.86 (0.14)	5.77	6.15 (0.13)	6.53 (0.35)	6.24 (0.30)
Na_2O	3.31 (0.19)	3.38	3.36 (0.15)	3.35 (0.17)	3.29 (0.14)
K_2O	3.73 (0.10)	3.31	3.48 (0.08)	3.30 (0.17)	3.48 (0.19)
P_2O_5	0.50 (0.01)	0.18	0.47 (0.02)	0.45 (0.02)	0.48 (0.03)
S	0.002 (0.002)	0.025	0.006 (0.003)	0.012 (0.009)	0.005 (0.002)
Cl	0.064 (0.009)	0.081	0.066 (0.005)	0.071 (0.006)	0.071 (0.005)
H_2O (SIMS/EPMA)	na/na	0.6/1.8	na/na	na/na	na/na
CO_2 (SIMS)	na	0.003	na	na	na
Temperature (°C)[a]					

Sample ID	2014.11.26–27 scoria								
	I141129S01				I141129S02			I141129S03	I141129S
	Groundmass bulk	Glass in groundmass	Glass in groundmass		Groundmass bulk	Glass in groundmass		Groundmass bulk	Glass in groundmass
	Av ($n=20$, 1 s)		Av ($n=20$, 1 s)		Av ($n=30$, 1 s)	Av ($n=20$, 1 s)		Av ($n=30$, 1 s)	
SiO_2	57.36 (0.57)	58.41	57.57 (0.47)		57.89 (2.25)	57.64 (0.67)		57.80 (0.87)	59.63
TiO_2	1.31 (0.04)	1.33	1.32 (0.02)		1.19 (0.33)	1.38 (0.03)		1.31 (0.13)	1.36
Al_2O_3	14.25 (0.34)	14.61	14.06 (0.11)		15.16 (2.49)	13.68 (0.23)		14.77 (0.93)	14.07
FeOt	9.35 (0.26)	9.40	9.15 (0.24)		8.74 (1.90)	9.42 (0.23)		9.25 (1.04)	10.06
MnO	0.19 (0.03)	0.18	0.18 (0.03)		0.17 (0.06)	0.19 (0.03)		0.18 (0.03)	0.22
MgO	2.79 (0.16)	2.84	2.78 (0.08)		2.76 (1.22)	2.48 (0.16)		2.63 (0.46)	2.56
CaO	6.00 (0.23)	6.00	5.89 (0.15)		6.08 (0.89)	5.62 (0.21)		6.11 (0.51)	6.07
Na_2O	3.11 (0.19)	3.34	3.01 (0.18)		3.32 (0.34)	2.85 (0.15)		3.20 (0.21)	3.43
K_2O	3.29 (0.14)	3.35	3.31 (0.09)		3.11 (0.56)	3.58 (0.16)		3.22 (0.29)	3.39
P_2O_5	0.22 (0.03)	0.47	0.24 (0.02)		0.20 (0.10)	0.26 (0.03)		0.22 (0.04)	0.50
S	0.006 (0.003)	0.001	0.006 (0.004)		0.005 (0.006)	0.003 (0.003)		0.006 (0.003)	0.006
Cl	0.062 (0.004)	0.054	0.060 (0.007)		0.029 (0.014)	0.067 (0.007)		0.064 (0.008)	0.068
H_2O (SIMS/EPMA)	na/na	0.1/nd	na/0.1	na/(0.1)	na/na	na/0.2	na/(0.2)	na/na	0.3/nd
CO_2 (SIMS)	na	nd	na		na	na		na	nd
Temperature (°C)[a]	1092				1069			1077	

FeOt, total FeO; nd, not detected; na, not analyzed

[a] Estimated from the chemical composition of the groundmass by glass (liquid) thermometer (Putirka 2008, Eq. (16)). This thermometer can apply to liquid in equilibrium with olivine + plagioclase + clinopyroxene + spinel (or oxides) and yields a standard error of estimate (SEE) of 26 °C. Pressure of 100 MPa was assumed

[b] Chemcial composition of glass in groundmass of ash particles erupted on July 10, 2003, is after GSJ et al. (2004)

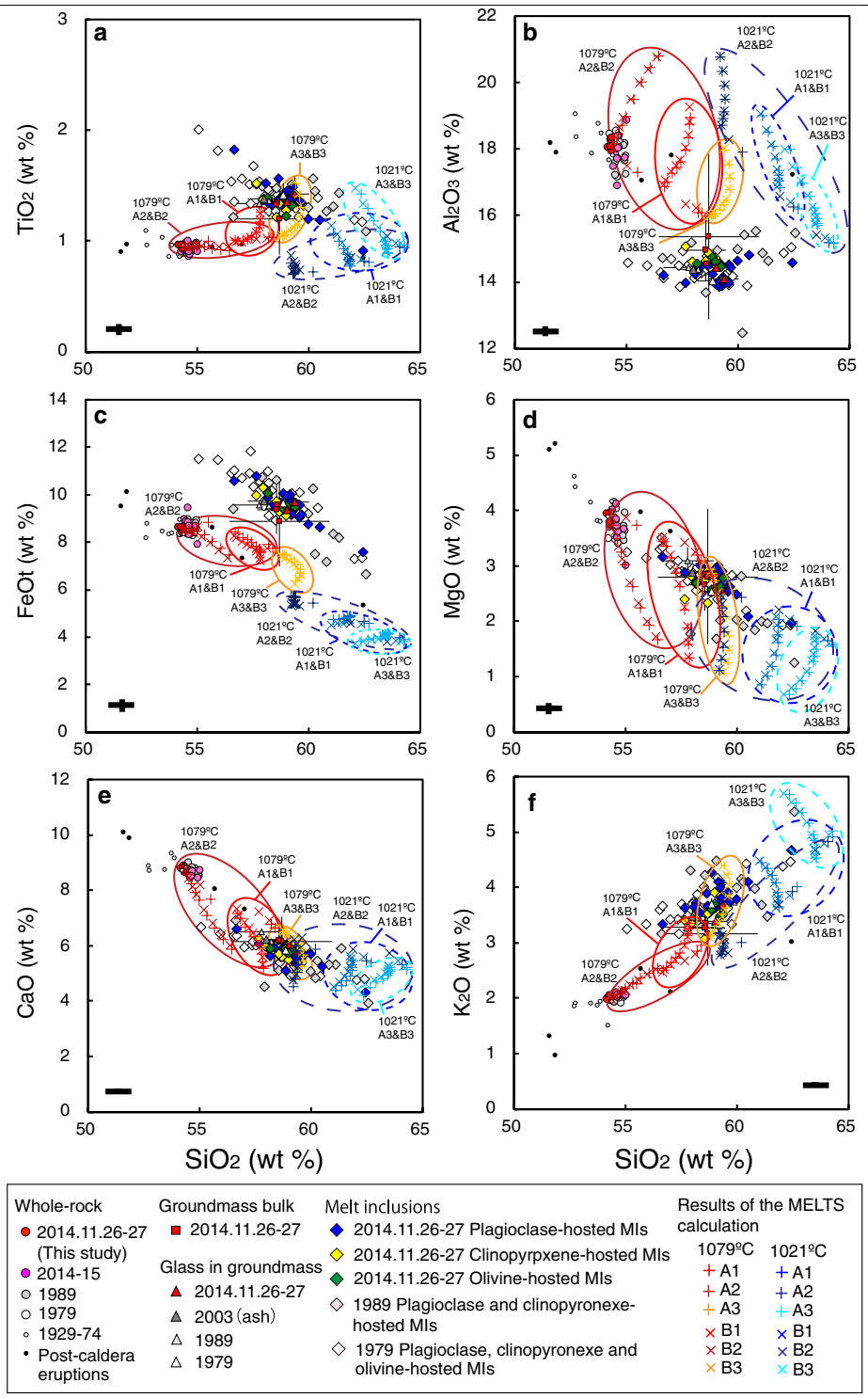

Fig. 2 The results of the major-element composition analysis of the eruptive products of the 1979–2014 eruptions. The major-element compositions of the whole-rock January 26–27, 2014, scoria, groundmass in the 1979, 1989, and 2014 scoria, and 2003 ash particles, and melt inclusions in the 1979, 1989, and 2014 scoria are shown. The analytical errors of the EPMA measurement (Saito et al. 2010) are shown as black bars in the lower part of each graph. The chemical compositions of the melt calculated from the whole-rock composition of I141129S01 using the MELTS program (Table 5; Additional file 3: Table S2) are also shown as cross symbols (see text). The whole-rock composition of the scoria erupted from 1929 to 1974 and from June to November 1979 (GSJ and Kumamoto Univ 1990; Ono and Watanabe 1985), scoria from October 1989 to November 1990 (GSJ and Kumamoto Univ 1990; Aso Volcano Museum et al. 1991), and scoria from November 2014 to March 2015 (NIED et al. 2015a, b) are also shown

plagioclases and clinopyroxenes in the 1989 scoria have a similar chemical composition of 57–63 wt% SiO_2 and 3.2–5.4 wt% K_2O (Fig. 2), as do those in the 2014 scoria, which have a composition of 58–62 wt% SiO_2 and 3.1–4.7 wt% K_2O. The similarity in the major-element compositions of the melt inclusions in the 1979, 1989, and 2014 scoria suggests that magma chamber conditions remained unchanged from 1979 to 2014. The chemical compositions of the inclusions in the 2014 scoria are similar to those of the groundmass bulk (Table 3; Fig. 2), indicating their inclusion entrapment immediately prior to the eruption.

The H_2O content of each inclusion determined by SIMS analysis was consistent with the content determined by EPMA and was within the large experimental error of the EPMA (±1 wt%). The melt inclusions in the 1979 scoria had volatile contents of 0.3–1.6 wt% H_2O (analyzed by SIMS), 0.007–0.034 wt% CO_2, and 0.010–0.035 wt% S (Table 3; Figs. 5 and 6). The melt inclusions in the 1989 scoria had 0.3–0.6 wt% H_2O (by SIMS), 0.003–0.009 wt% CO_2, and 0.008–0.031 wt% S, which agree with the volatile contents of the inclusions in the 1979 scoria, within experimental error (±0.2 wt% H_2O by SIMS, ±0.0028 wt% CO_2, and ±0.007 wt% S). The melt inclusions in the 2014 scoria have volatile contents of 0.6–0.8 wt% H_2O (by SIMS), 0.003–0.017 wt% CO_2, and 0.008–0.036 wt% S (Table 3; Figs. 5 and 6), which are similar to those of the 1979 and 1989 scoria. The similarity of the volatile content of the melt inclusions among these eruptions suggests that the volatile content of the magma in the magma chamber did not change from 1979 to 2014. Tamura et al. (2015) reported similar volatile contents of the melt inclusions in bombs of Nakadake (0.4–1.6 wt% H_2O and 0.01–0.02 wt% S), although the eruption time of the bomb was not determined.

The large variability in CO_2 and S content of the melt inclusions in the 1979, 1989, and 2014 scoria is not related to the K_2O content (Fig. 5), suggesting either the addition of volatiles or magma degassing with pressure decrease. The distribution of H_2O and CO_2 content of the inclusions (Fig. 6a) suggests magma degassing with pressure decrease (Fig. 6e). The mass ratios of CO_2/H_2O, CO_2/S, and S/H_2O in the type A and B gases emitted on January 12, 2015, were calculated from the known molar ratios of type A and B gases, assuming that SO_2 is the only S species in the gas (solid and dashed lines in Fig. 6). The CO_2/H_2O and CO_2/S ratios of the melt inclusions in the 1979, 1989, and 2014 scoria were lower than those in the volcanic gases, except for three inclusions in the 1979 scoria that had high CO_2/S ratios (Fig. 6a, b). In addition, most of the melt inclusions analyzed for H_2O by SIMS had lower S/H_2O ratios than the volcanic gases, except for two inclusions in the 1979 and 1989 scoria (Fig. 6c). These disagreements between the CO_2/H_2O, CO_2/S, and S/H_2O ratios of the inclusions and those of the volcanic gas reflect the high variability of CO_2 and S contents of the melt inclusions (Fig. 6). The large variation in CO_2 and S content of the melt inclusions with almost constant K_2O content (Fig. 5) indicates that crystallization of melt did not cause the variations. This indicates that the inconsistencies are likely a result of exsolution of CO_2 and S from the melt prior to inclusion entrapment.

Temperature and pressure of magma

We estimated the magma temperature using a glass (liquid) thermometer for a melt in equilibrium with olivine + plagioclase + clinopyroxene [Eq. (16) in Putirka 2008]. Based on the chemical compositions of the groundmass bulk in the three 2014 scoria, temperatures of 1092 °C, 1069 °C, and 1077 °C were obtained, assuming a pressure of 100 MPa (Table 4). We also applied the olivine–liquid and plagioclase–liquid thermometers and the clinopyroxene–liquid thermobarometer (Putirka 2008) to chemical compositions of the rims of phenocrysts and the groundmass bulk in the 2014 scoria, resulting in the temperatures ranging from 1042 to 1090 °C and the pressures ranging from 250 to 570 MPa (Additional file 2: Table S1). These temperature estimates were nearly identical to those obtained by the glass thermometer (1069–1092 °C), considering the standard errors of the estimate determined by Putirka (2008; ±26 °C, ±29 °C, and ±36 °C for the glass, olivine–liquid, and plagioclase–liquid thermometers, respectively, and ±42 °C for the clinopyroxene–liquid thermobarometer). Taking this evidence into account, we concluded that the magma from the 2014 eruption likely had a temperature of 1042–1092 °C.

Similarly, we applied the thermometers and thermobarometers to the chemical compositions of the melt and their host phenocrysts of olivine-, plagioclase-, and clinopyroxene-hosted melt inclusions from the 1979, 1989, and 2014 scoria and obtained temperatures of 1034–1074 °C (average of 1059 °C with standard deviation of ±15 °C) and pressures of 390–560 MPa (average of 450 MPa with standard deviation of 76 MPa) for the 1979 scoria, 1031–1071 °C (average of 1057 °C with standard deviation of ±16 °C) and 280–560 MPa (average of 442 MPa with standard deviation of 102 MPa) for the 1989 scoria, and 1027–1081 °C (average of 1056 °C with standard deviation of ±19 °C) and 420–460 MPa (average of 440 MPa with a range of 20 MPa) for the 2014 scoria (Table 3). Theses temperature and pressure estimates for the melt inclusions in the 2014 scoria were similar to those of the groundmass bulk and the phenocryst rims (1042–1092 °C and 250–570 MPa). In addition, the temperature and pressure estimates of the melt inclusions of 1979, 1989, and 2014 scoria are consistent within their

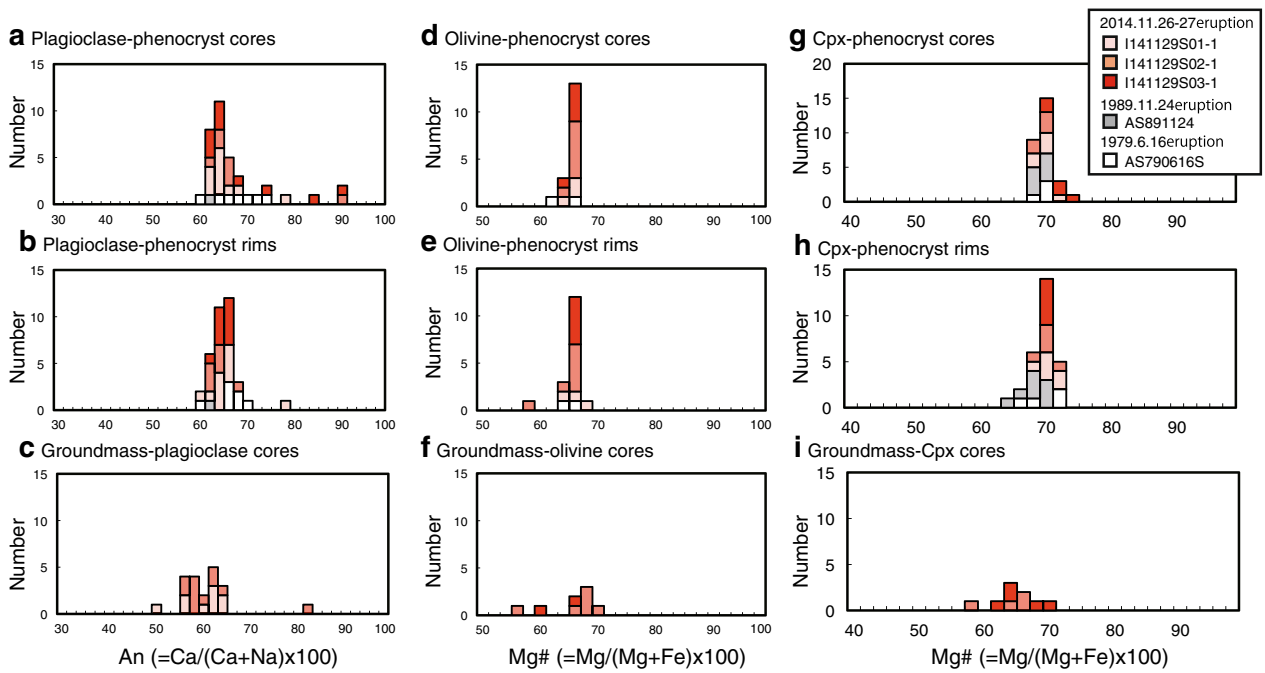

Fig. 3 Chemistry of phenocrysts and groundmass minerals in the 1979, 1989, and 2014 scoria. Repeated analyses of reference minerals of plagioclase, augite, and olivine indicated precision of An ±0.7 for the plagioclase (An67.1), Mg# ±0.3 for the augite (Mg# 87.1), and Mg# ±0.1 for the olivine (Fo90.5) (Saito et al. 2002)

standard deviations. Therefore, in the discussion that follows, we will use the average temperature estimate from the glass thermometry for the 2014 scoria (1079 °C with standard deviation of 12 °C) for the temperature of the magma erupted in 1979–2014. In addition, we will use 600 MPa as a maximum pressure of the magma in our MELTS calculation (Table 5; Additional file 3: Table S2).

The variation in CO_2 and S content of the inclusions in conjunction with the major-element compositions staying consistent (Fig. 5b, c), and the distribution of H_2O and CO_2 content in the inclusions (Fig. 6a), suggests that the cause of the variability in CO_2 and S content is a pressure decrease in the magma (Fig. 6e). Gas saturation pressures ranging from 51 to 118 MPa were obtained using the H_2O and CO_2 content of four inclusions in the 1979 scoria in the solubility model proposed by Papale et al. (2006) for andesite magmas (Table 3; Fig. 6a). This pressure range corresponds to a depth of 2–4 km under a lithostatic pressure gradient. The H_2O and CO_2 content of five inclusions in the 1989 scoria yielded a lower gas saturation pressure range of 18–50 MPa (Table 3; Fig. 6a), which corresponds to a depth of 1–2 km. The H_2O and CO_2 content of five inclusions in the 2014 scoria yielded a gas saturation pressure range of 22–80 MPa (Table 3; Fig. 6a), which corresponds to a depth of 1–3 km.

The tomographic inversions for P- and S-velocity structure (Sudo and Kong 2001) and the three-dimensional modeling of the electrical resistivity structure (Hata et al. 2016) beneath the Aso caldera indicate the presence of a magma chamber at 2–10 km depth (bsl; Fig. 7). In addition, the spatial pattern of the observed long-period tremors (Yamamoto et al. 1999) and the three-dimensional modeling of the electrical resistivity structure (Hata et al. 2016) suggest the existence of a conduit from 4 km depth (bsl) to 0 km depth (bsl; Fig. 7). Four inclusions of the 1979 scoria and one inclusion of the 2014 scoria that yielded gas saturation pressures of 80–118 MPa (corresponding to depths of 3–4 km) were trapped in their host phenocrysts at the upper part of the magma chamber or the lower part of the conduit at depths of 2–3 km (bsl). Two inclusions of the 1979 scoria, six inclusions of the 1989 scoria, and four inclusions of the 2014 scoria that yielded gas saturation pressures of 18–61 MPa (corresponds to depth of 1–2 km) were trapped in their host phenocrysts at the conduit at depth of 0–1 km (bsl). These results suggest that the melt inclusion entrapments occurred in a conduit during the magma ascent. Such inclusion entrapment during a magma ascent was also proposed for the 2000 eruption at Miyakejima volcano (Saito et al. 2005).

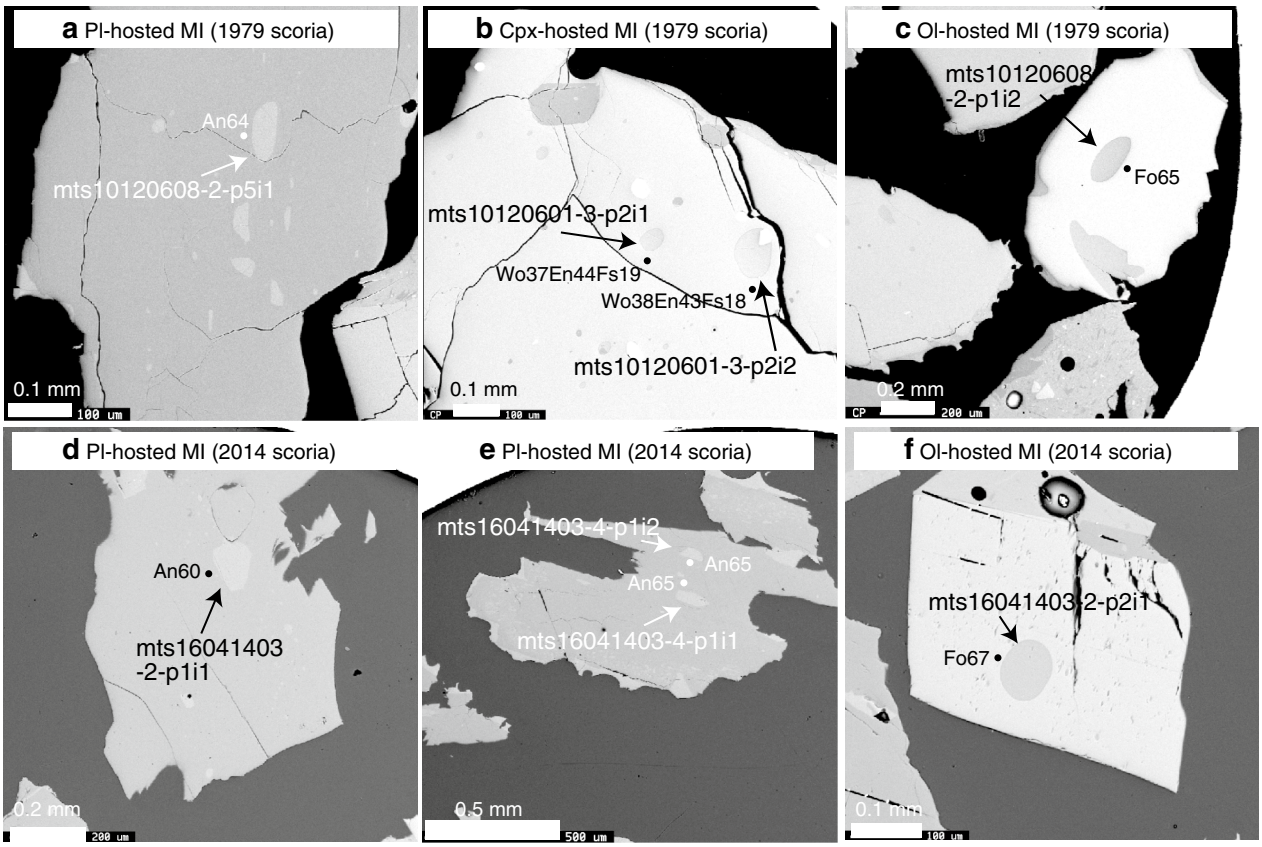

Fig. 4 Backscattered electron images of the melt inclusions contained in the 1979 and 2014 scoria. **a** A plagioclase-hosted melt inclusion in the 1979 scoria (mts10120608-2-p5i1). **b** Clinopyroxene-hosted melt inclusions in the 1979 scoria (mts10120601-3-p2i1 and p2i2). **c** An olivine-hosted melt inclusion in the 1979 scoria (mts10120608-2-p1i2). **d** A plagioclase-hosted melt inclusion in the 2014 scoria (mts16041403-2-p1i1). **e** Plagioclase-hosted melt inclusions in the 2014 scoria (mts16041403-4-p1i1 and p1i2). **f** An olivine-hosted melt inclusion in the 2014 scoria (mts16041403-2-p2i1)

Bulk volatile content and density of magma

The CO_2/H_2O and S/H_2O mass ratios of the inclusions were lower than those of the volcanic gas (Fig. 6a, c). Two possible explanations for the disagreement should be considered: (1) different origins of the volcanic gas and the melt inclusions and (2) supersaturation of CO_2 and S at the time of inclusion entrapment. However, the former explanation is unlikely because the scoria specimens that erupted from November 26–27, 2014, to March 26, 2015 (Fig. 2 a, b; GSJ 2015b; NIED et al. 2015a, b), have identical whole-rock compositions, supporting the idea that the volatiles released by the magma on January 12, 2015, were somehow similar to those that erupted on November 26–27, 2014. Therefore, the disagreement of the mass ratios of CO_2/H_2O and S/H_2O between the inclusions and the volcanic gas (Fig. 6) is most likely due to the supersaturation of CO_2 and S at the time of inclusion entrapment.

The above discussion indicates that only measurements of the melt inclusions might cause underestimation of total volatile content of the magmas, especially regarding less dissolved volatile species such as CO_2 (Papale 2005). In order to estimate the total volatile content of the magmas, we calculated the bulk CO_2 and S content of the magma, assuming that entrapment of the inclusions occurred under supersaturation of CO_2 and S and that the magma emitted volcanic gases of types A and B. The H_2O content of the degassed magma after volcanic gas emission was assumed to be 0.12 wt% based on the average H_2O content of groundmass glass (0.2 wt%; Table 4) and assuming a glass content of 60 wt%. The CO_2 content of the degassed magma was assumed to be 0 wt% and the S content was assumed to be 0.006 wt% based on the average S content of the groundmass bulk of three 2014 scoria specimens (Table 4). A bulk H_2O content of 1 wt% for the pre-eruptive magma was obtained, given the maximum possible H_2O content of the inclusion (1.6 wt%; value obtained for inclusion mts10120608-2-p1i1 by SIMS; Table 3) and groundmass content in the scoria (60 wt%; Table 2). On the basis of the above

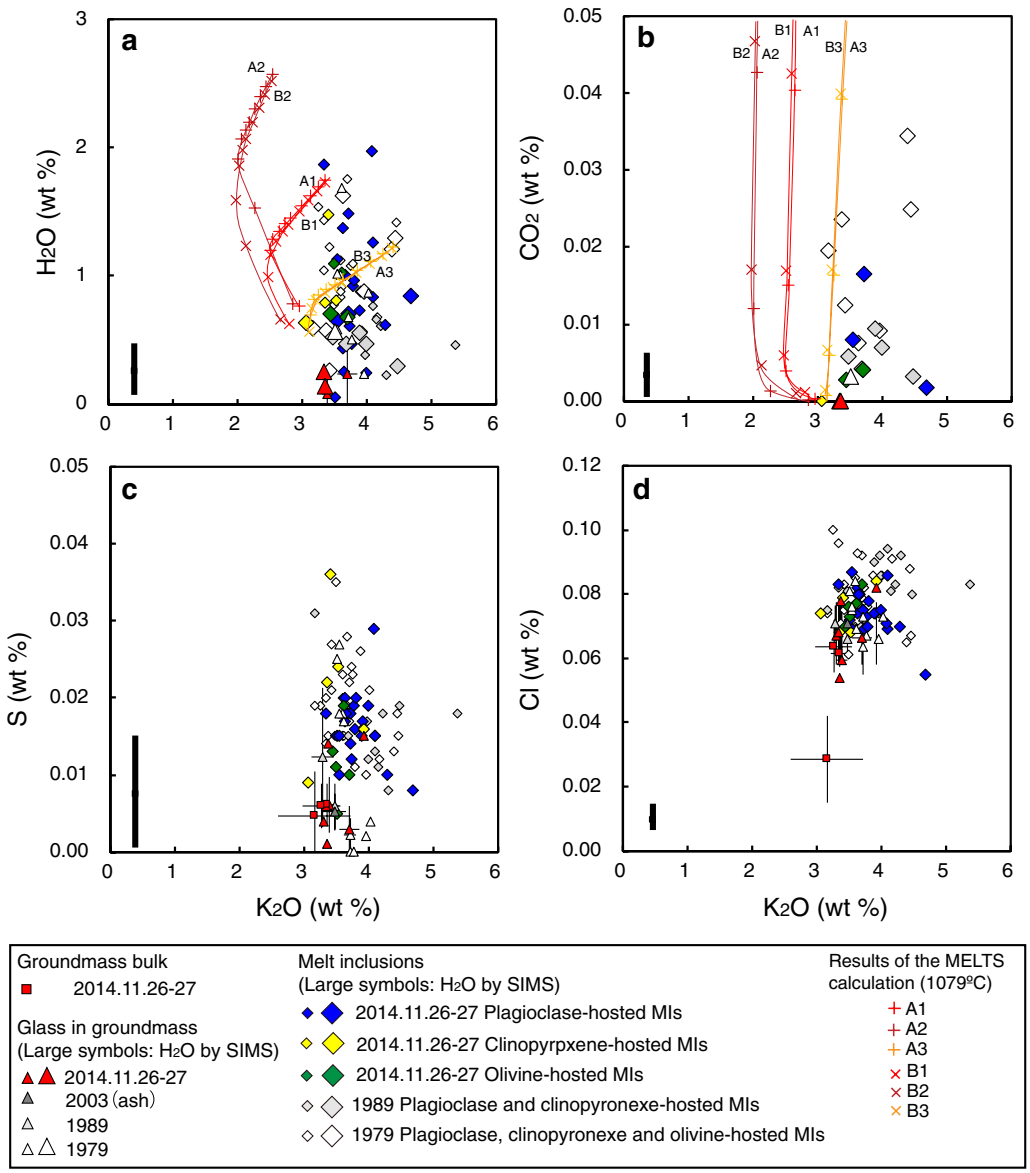

Fig. 5 Volatile and K_2O contents of the melt inclusions and groundmass in the scoria. **a** H_2O and K_2O contents, **b** CO_2 and K_2O contents, **c** S and K_2O contents, and **d** Cl and K_2O contents of the melt inclusions and groundmass. The large symbols indicate H_2O and CO_2 contents measured by SIMS. Error bars indicate the analytical errors of H_2O and CO_2 by SIMS and those of S, Cl, and K_2O by EPMA. The EPMA analytical error of H_2O is ± 1 wt%. Chemical compositions of the melt calculated from the whole-rock composition of I141129S01 at 1079 °C using the MELTS program (Table 5; Additional file 3: Table S2) are also shown. Curves with cross symbols show the compositional change associated with a decrease in pressure from 600 to 10 MPa

assumptions, we calculated bulk CO_2 and S content in the magma to be 0.09 and 0.07 wt% from the mass ratios of CO_2/H_2O and S/H_2O in the type A gas ("A1 magma" in Table 6). If type B gas was emitted from the magma, the bulk CO_2 and S content in the magma were calculated to be 0.5 and 0.04 wt% ("B1 magma"). We also performed the calculation for 2 wt% H_2O content, as that represents the maximum estimated H_2O content. The calculation yielded bulk CO_2 and S content in the magma of 0.18 wt% CO_2 and 0.08 wt% S for the type A gas ("A2 magma" in Table 6) and 1 wt% CO_2 and 0.08 wt% S for the type B gas ("B2 magma" in Table 6). Finally, we performed the calculation for a bulk H_2O content of 0.5 wt%, matching the H_2O content of the inclusion of the 2014 scoria (0.8 wt%; determined by SIMS for inclusion mts16041403-2-p1i1; Table 3). The calculation yielded bulk CO_2 and S content

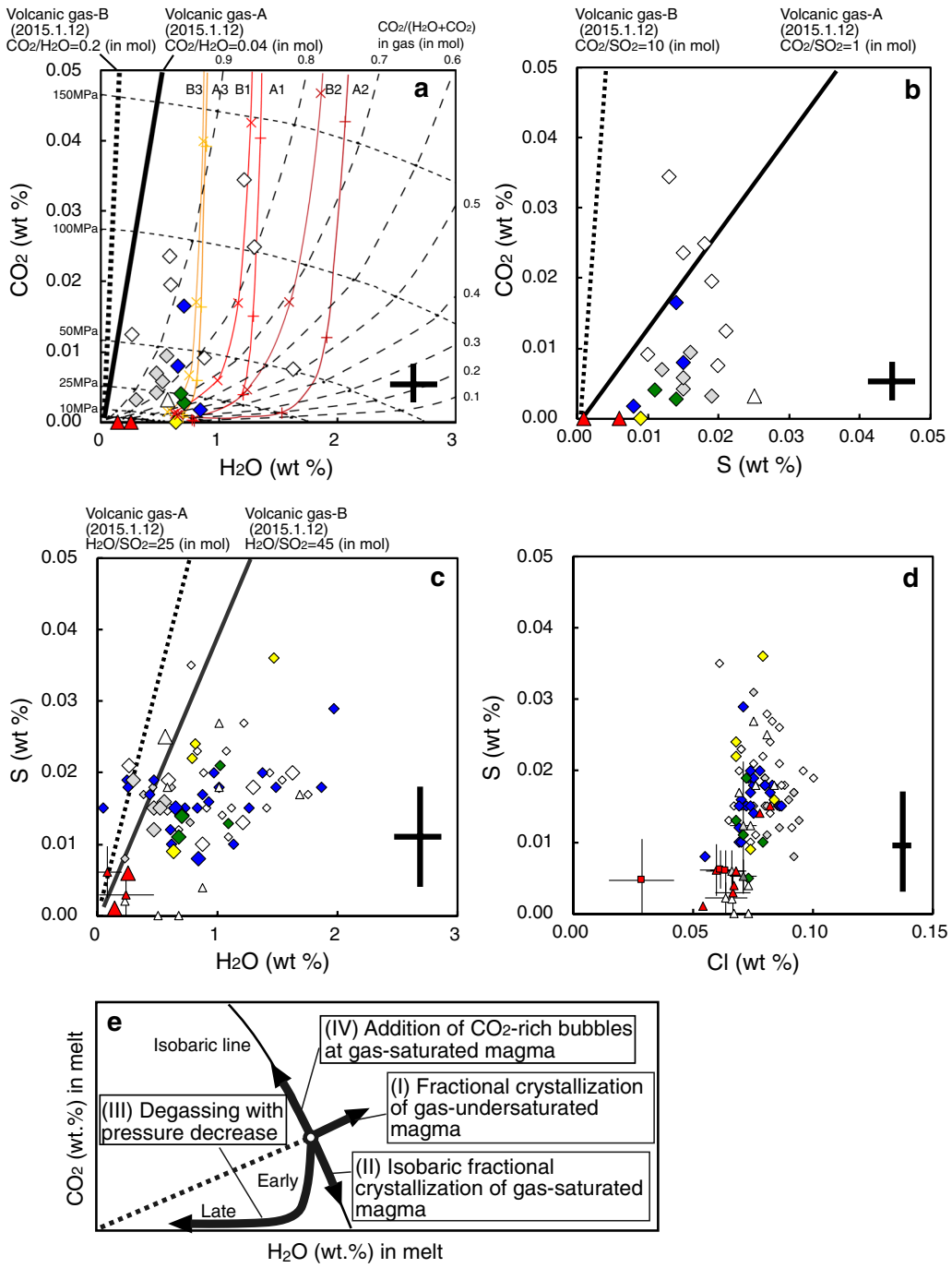

Fig. 6 Volatile content of melt inclusions and glass in the groundmass in the scoria. The CO_2/H_2O, CO_2/SO_2, and H_2O/SO_2 ratios of the volcanic gases are shown as solid lines (type A) and dashed lines (type B). **a** H_2O and CO_2 content of the melt inclusions analyzed by SIMS. H_2O and CO_2 contents of the melt of the A1, A2, A3, B1, B2, and B3 magmas calculated by MELTS at 1079 °C (Table 5; Additional file 3: Table S2) are also shown. **b** S and CO_2 contents of the melt inclusions. **c** H_2O and S contents of the melt inclusions. **d** Cl and S contents of the melt inclusions. **e** Possible evolution processes of H_2O and CO_2 in a magma chamber for (I) fractional crystallization of gas-undersaturated magma, (II) isobaric fractional crystallization of gas-saturated magma, (III) degassing with pressure decrease, and (IV) addition of CO_2-rich bubbles to gas-saturated magma (Saito et al. 2001). Process (III) causes an initial drastic decrease in CO_2 concentration (as shown by "Early"), which is followed by a decrease in H_2O concentration (as shown by "Late") because of the lower solubility of CO_2 compared with H_2O. The symbols are the same as in Fig. 5. Error bars indicate the analytical errors of H_2O and CO_2 by SIMS and those of S and Cl by EPMA. The analytical error of H_2O by EPMA in (**c**) is ±1 wt%

Table 5 Representative results of calculations of MELTS, densities, and volumes of bubbles of the magmas. The calculations were done for six types of magmas (A1, A2, A3, B1, B2, and B3) at a temperature of 1079 °C

Magma	A1	A1	A1	A1	A1	A2	A2	A2	A2	A2	A3	A3	A3	A3	A3
Bulk H_2O (wt%)	1	1	1	1	1	2	2	2	2	2	0.5	0.5	0.5	0.5	0.5
Temperature (°C)	1079	1079	1079	1079	1079	1079	1079	1079	1079	1079	1079	1079	1079	1079	1079
Pressure (MPa)	400	200	100	50	25	400	200	100	50	25	400	200	100	50	25
Phase (vol%)[b]															
Melt	65.6	72.3	76.9	79.2	80.4	87.0	92.5	96.1	98.2	88.3	48.9	55.5	59.8	62.4	63.7
Plagioclase (An)	17.9 (63)	15.8 (68)	14.1 (71)	13.4 (72)	13.2 (73)	0.2 (74)	0.6 (79)	0.4 (81)	0.2 (82)	7.7 (77)	31.8 (56)	29.0 (60)	26.8 (63)	25.5 (64)	24.9 (65)
Olivine (Fo)	0.0	0.0	0.0	0.2 (73)	0.5 (74)	0.0	0.0	0.0	0.0	0.0	0.0	0.0	0.0	0.0	0.0
Clinopyroxene (Mg#)	15.8 (64)	10.8 (69)	8.0 (71)	6.2 (72)	5.1 (73)	12.8 (67)	6.9 (70)	3.5 (73)	1.6 (73)	3.7 (74)	18.1 (62)	13.8 (67)	11.5 (69)	10.2 (70)	9.6 (71)
Orthopyroxene (Mg#)	0.0	0.0	0.0	0.0	0.0	0.0	0.0	0.0	0.0	0.0	0.0	0.0	0.0	0.0	0.0
Spinel	0.7	1.0	1.1	1.0	0.9	0.0	0.0	0.0	0.0	0.3	1.3	1.7	1.8	1.8	1.8
Chemical composition of melt (wt%)															
SiO_2	57.8	57.4	57.0	56.8	56.7	55.7	55.0	54.6	54.5	55.5	59.7	59.5	59.2	59.0	58.9
TiO_2	1.1	1.0	1.0	1.0	1.0	0.9	0.9	0.9	0.9	1.0	1.3	1.1	1.1	1.1	1.1
Al_2O_3	18.3	17.6	17.3	17.0	16.9	20.0	19.0	18.4	18.2	17.3	17.1	16.5	16.2	16.0	16.0
FeOt	7.7	8.0	8.2	8.3	8.4	8.0	8.5	8.6	8.6	8.8	6.7	7.1	7.3	7.4	7.5
MnO	0.3	0.2	0.2	0.2	0.2	0.2	0.2	0.2	0.2	0.2	0.4	0.3	0.3	0.3	0.3
MgO	1.9	2.6	3.1	3.4	3.4	2.2	3.0	3.5	3.7	3.7	1.5	2.1	2.5	2.7	2.9
CaO	5.7	6.3	6.7	7.0	7.2	6.6	7.6	8.2	8.6	7.7	5.4	5.9	6.2	6.4	6.4
Na_2O	3.6	3.5	3.4	3.4	3.3	3.5	3.3	3.2	3.1	3.2	3.2	3.3	3.4	3.4	3.4
K_2O	3.1	2.8	2.6	2.5	2.5	2.4	2.2	2.1	2.0	2.3	4.1	3.6	3.4	3.2	3.2
P_2O_5	0.5	0.4	0.4	0.4	0.4	0.3	0.3	0.3	0.3	0.3	0.6	0.5	0.5	0.5	0.5
H_2O[c]	1.6	1.5	1.3	1.3	1.2	2.4	2.2	2.1	1.9	1.5	1.1	1.0	0.9	0.8	0.8
CO_2[c]	0.146	0.098	0.040	0.015	0.004	0.215	0.113	0.043	0.012	0.001	0.089	0.078	0.039	0.016	0.006
Gas (wt%)[d]	0.00	0.04	0.09	0.13	0.20	0.00	0.10	0.19	0.31	1.00	0.00	0.00	0.04	0.06	0.08
H_2O in gas (in mol)[d]		0.15	0.24	0.39	0.67		0.27	0.42	0.67	0.90			0.14	0.24	0.43
Volume of bubbles (vol%)[d]	0.00	0.13	0.64	1.85	6.67	0.00	0.50	1.81	6.51	33.48	0.00	0.00	0.18	0.60	1.78
Density (kg m^{-3})[d]	2696	2632	2586	2531	2400	2623	2536	2458	2320	1704	2743	2692	2662	2633	2594
Magma	**B1**	**B1**	**B1**	**B1**	**B1**	**B2**	**B2**	**B2**	**B2**	**B2**	**B3**	**B3**	**B3**	**B3**	**B3**
Bulk H_2O (wt%)	1	1	1	1	1	2	2	2	2	2	0.5	0.5	0.5	0.5	0.5
Temperature (°C)	1079	1079	1079	1079	1079	1079	1079	1079	1079	1079	1079	1079	1079	1079	1079
Pressure (MPa)	400	200	100	50	25	400	200	100	50	25	400	200	100	50	25
Phase (vol%)[b]															
Melt	66.3	73.3	78.0	80.3	81.5	87.7	93.9	97.5	99.4	93.1	49.2	56.0	60.4	63.0	64.3
Plagioclase (An)	17.4 (63)	15.2 (68)	13.3 (71)	12.7 (72)	12.5 (73)	0.0	0.0	0.0	0.0	4.7 (78)	31.5 (56)	28.6 (60)	26.4 (63)	25.2 (64)	24.5 (65)

Table 5 (continued)

Magma	B1	B1	B1	B1	B1	B2	B2	B2	B2	B2	B3	B3	B3	B3	B3
Olivine (Fo)	0.0	0.0	0.0	0.2 (73)	0.4 (74)	0.0	0.0	0.0	0.0	0.0	0.0	0.0	0.0	0.0	0.0
Clinopyroxene (Mg#)	15.5 (63)	10.5 (69)	7.6 (71)	5.8 (72)	4.6 (73)	12.3 (65)	6.1 (70)	2.5 (73)	0.6 (74)	2.0 (72)	18.0 (61)	13.7 (66)	11.4 (69)	10.0 (70)	9.4 (71)
Orthopyroxene (Mg#)	0.0	0.0	0.0	0.0	0.0	0.0	0.0	0.0	0.0	0.0	0.0	0.0	0.0	0.0	0.0
Spinel	0.8	1.1	1.1	1.0	0.9	0.0	0.0	0.0	0.0	0.2	1.3	1.7	1.8	1.9	1.9
Chemical composition of melt (wt%)															
SiO_2	57.8	57.4	57.0	56.8	56.6	55.6	54.8	54.5	54.4	55.0	59.6	59.4	59.2	58.9	58.8
TiO_2	1.1	1.0	1.0	1.0	1.0	1.0	1.0	0.9	0.9	1.0	1.3	1.2	1.1	1.1	1.1
Al_2O_3	18.4	17.7	17.3	17.1	16.9	20.0	19.0	18.4	18.0	17.5	17.2	16.5	16.2	16.1	16.0
FeOt	7.5	7.8	8.0	8.2	8.3	8.0	8.4	8.5	8.5	8.7	6.6	7.0	7.2	7.4	7.4
MnO	0.3	0.2	0.2	0.2	0.2	0.2	0.2	0.2	0.2	0.2	0.4	0.3	0.3	0.3	0.3
MgO	1.9	2.7	3.2	3.4	3.5	2.3	3.1	3.6	3.9	3.9	1.5	2.1	2.5	2.8	2.9
CaO	5.9	6.5	6.8	7.1	7.3	6.8	7.8	8.4	8.8	8.2	5.5	6.0	6.3	6.4	6.5
Na_2O	3.6	3.5	3.4	3.3	3.3	3.5	3.3	3.1	3.0	3.1	3.2	3.3	3.4	3.4	3.4
K_2O	3.1	2.8	2.6	2.5	2.5	2.3	2.1	2.0	2.0	2.1	4.0	3.6	3.4	3.2	3.1
P_2O_5	0.5	0.4	0.4	0.4	0.4	0.3	0.3	0.3	0.3	0.3	0.6	0.5	0.5	0.5	0.5
H_2O^c	1.6	1.4	1.3	1.2	1.0	2.3	2.1	1.9	1.6	1.2	1.1	1.0	0.9	0.8	0.7
CO_2^c	0.245	0.102	0.043	0.017	0.006	0.289	0.118	0.047	0.017	0.005	0.224	0.093	0.040	0.017	0.007
Gas (wt%)[d]	0.59	0.66	0.70	0.77	0.91	0.97	1.10	1.22	1.43	2.04	0.22	0.30	0.34	0.36	0.41
H_2O in gas (in mol)[d]	0.11	0.15	0.22	0.35	0.53	0.17	0.24	0.36	0.52	0.69	0.07	0.09	0.14	0.23	0.38
Volume of bubbles (vol%)[d]	1.33	2.48	4.74	9.95	22.52	2.97	5.40	10.55	22.60	46.51	0.37	0.86	1.73	3.60	8.33
Density (kg m^{-3})[d]	2676	2586	2494	2345	2007	2579	2444	2272	1959	1378	2740	2681	2630	2562	2430

See Additional file 4: Table S3 for detail calculation procedures

FeOt, total FeO

[a] Bulk CO_2 and S contents of the magmas before degassing are given in Table 6

[b] Values in parenthesis show chemical composition of the minerals. An, anorthite content (mol%) in plagioclase (An/(An + Ab) × 100%), Fo, forsterite content (mol%) in olivine, Mg#, Mg/(Mg + Fe) × 100%

[c] Water and CO_2 contents of the melt were calculated from the pressure, temperature chemical composition of the melt and the bulk H_2O and CO_2 contents using the solubility model of Papale et al. (2006)

[d] Gas contents ($H_2O + CO_2$, wt%) of the fluid (melt and gas) and mol fractions of H_2O in the gases were calculated from the pressure, temperature chemical composition of the melts, and the bulk H_2O and CO_2 contents of the fluids using the solubility model of Papale et al. (2006). The volumes of bubbles were calculated from the masses of H_2O and CO_2 gases exsolved from the melt and densities of H_2O and CO_2 gases that were calculated with Modified Redlich–Kwong equation of state (Holloway 1981) . The densities of the magmas were calculated from the bubble volumes and masses and densities of the melt and crystal calculated by MELTS, assuming that the bubbles do not separate from the magma

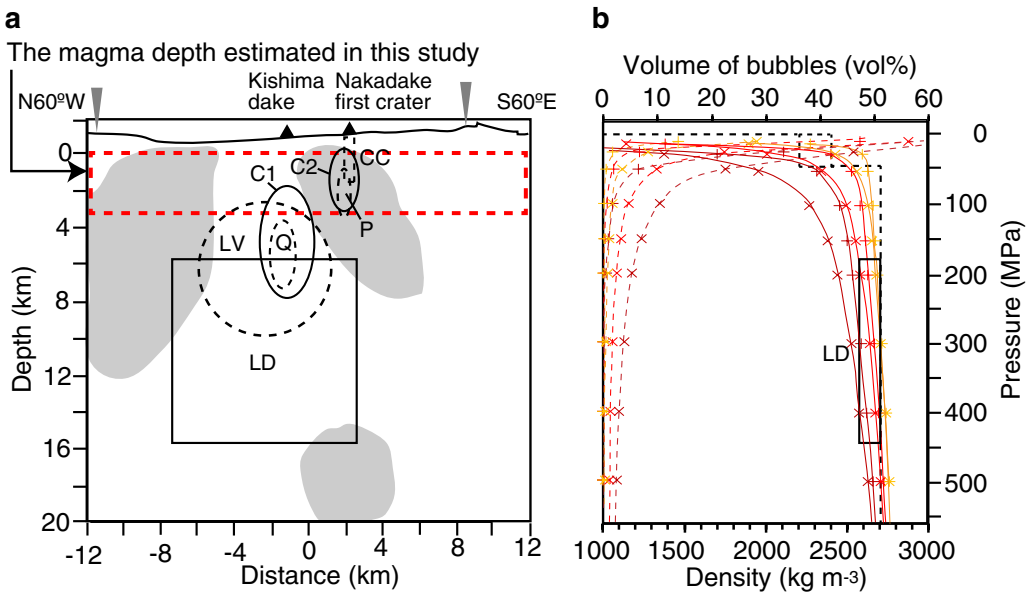

Fig. 7 A cross section of Aso caldera and results of a density calculation of magma. **a** Comparison of the magma depth estimated in this study with geophysical observations. This cross section is along the profile in Fig. 1 (profile A2 in Hata et al. 2016). The magma chambers and conduits proposed by geophysical observations are also shown. LD is a low-density cylindrical block with a density contrast of 150 kg m^{-3}, which is lower than that of the surrounding rocks, and is located at 6–17 km depth (bsl) with a radius of 5 km (Komazawa 1995). LV is a low-velocity region that is roughly spherical in shape, has a radius of about 3 km, is centered at 6 km depth, and extends to 10 km depth (Sudo and Kong 2001). P and Q are hot regions, that is, reflector voids revealed by a 3-D seismic reflection analysis (Tsutsui and Sudo 2004). CC is a crack-like conduit with a dimension of 1 km at a depth of about 1.8 km (bsl) beneath the Nakadake first crater based on the spatial pattern of the observed long-period tremors amplitudes (Yamamoto et al. 1999). C1 and C2 are a magma chamber and a conduit, respectively, inferred from significant conductive block anomalies indicated by the three-dimensional modeling of the electrical resistivity structure (Hata et al. 2016). A portion with less than 10 O-m of the anomaly C1, whose most conductive cell at 4 km depth (bsl) indicated a melt fraction of 76–87%, was distributed from 8 to 2 km depth (bsl). The horizontal of the anomaly C1 is beneath Kishimadake, which is consistent with the estimate of Sudo and Kong (2001). The anomaly C2 is centered at 2 km depth (bsl) and ranges from 4 to 0 km. Gray areas indicate JMA earthquake hypocenters within 2 km of the profile line between June 2002 and April 2016 (Hata et al. 2016). These geophysical observations indicate the presence of a magma chamber at 2–10 km depth (bsl). **b** Density (solid curves) and volume of bubbles (broken curves) of the A1, A2, A3, B1, B2, and B3 magmas calculated in this study (Table 5; Additional file 3: Table S2). The symbols are the same as in Fig. 5. Black broken lines indicate the density structure beneath the Aso caldera investigated by Komazawa (1995). He estimated the density structure to be 2200–2400 kg m^{-3} at a depth less than 1 km (bsl) and 2700 kg m^{-3} at a depth greater than 1 km. LD is a low-density block with a density contrast of 150 kg m^{-3} extended from 6 to 17 km depth (bsl) proposed by Komazawa (1995). Comparison between the bulk densities of the A1, B1, A3, and B3 magmas and the density of the crust at different depths indicated. (1) At 200–600 MPa (6–21 km depth (bsl)), the A1, B1, A3, and B3 magmas had lower or similar bulk density (2586–2787 kg m^{-3}) than the crust (Additional file 3: Table S2). The density contrast between the A1 and B1 magmas and crust at 200 MPa was 68–114 kg m^{-3}, which was similar to the indication from the gravimetric analysis. (2) At pressures of 50–200 MPa (1–6 km depth (bsl)), the magmas had lower bulk densities than the crust (2345–2632 kg m^{-3} for A1 and B1 magmas and 2562–2692 kg m^{-3} for A3 and B3 magmas; Table 5; Additional file 3: Table S2), which would allow the magmas to ascend by buoyancy. (3) At a pressure of 25 MPa (0 km depth (bsl), the B1 magma had lower bulk density than the crust (2007 kg m^{-3} for B1 magma versus 2200–2400 kg m^{-3} for the crust), while the A1, A3, and B3 magmas had higher or similar bulk density (2400–2594 kg m^{-3}) to the crust

in the magma of 0.04 wt% CO_2 and 0.03 wt% S for the type A gas ("A3 magma" in Table 6) and 0.2 wt% CO_2 and 0.02 wt.% S for the type B gas ("B3 magma" in Table 6).

We applied the MELTS calculation using the whole-rock composition of the scoria (No. I141129S01 in Table 1), with a temperature of 1079 °C and NNO buffer to investigate whether the estimated bulk H_2O content (A1–A3, B1–B3) could reconstruct the mode composition of the 2014 scoria and the chemical composition of the melt inclusions (Table 5; Additional file 3: Table S2). The MELTS calculation for A1, B1, A3, and B3 magmas yielded similar mode composition of the scoria and similar chemical composition of the melt inclusions (see Additional file 3: Table S2; Table 5; Fig. 2), indicating that the bulk H_2O content of the magma was likely between 0.5 and 1 wt%. We also calculated the H_2O and CO_2 content of the melt in the magmas at each pressure using the solubility model of Papale et al. (2006) (Figs. 5 and 6). The relationships of H_2O and CO_2 content with K_2O content predicted by the MELTS calculation for A1

Table 6 Bulk volatile contents of magmas and amounts of degassed magma estimated from the chemical composition of the volcanic gas, emission rate of SO_2, and volatile content of the melt inclusions and the groundmass

Magma	Volcanic gas[a]		Bulk volatile content of magma[b]						Averaged emission rate of sulfur in 2014–2017[c]	Degassing rate	Magma degassed in 2014–2017[d]		Tephra in 2014–2016[e]		Magma degassed in 1979–2017[f]	
	CO_2/SO_2	H_2O/SO_2	Degassed magma			Magma before degassing										
			H_2O	CO_2	S	H_2O	CO_2	S			Mass	Volume	Mass	Volume	Mass	Volume
	(mol mol^{-1})	(mol mol^{-1})	(wt%)	(wt%)	(wt%)	(wt%)	(wt%)	(wt%)	(kg s^{-1})	(10^3 kg s^{-1})	(10^9 kg)	(10^9m^3 DRE)	(10^9 kg)	(10^9m^3 DRE)	(10^9 kg)	(10^9m^3 DRE)
A1	1	25	0.12	0	0.004	1	0.09	0.07	8.7 (±7.2)	13	1700	0.62	2.8	0.0010	3000	1.1
A2						2	0.18	0.14		6.4	810	0.30			1400	0.53
A3						0.5	0.04	0.03		33	4200	1.6			7500	2.8
B1	10	45				1	0.5	0.04		24	3000	1.1			5400	2.0
B2						2	1	0.08		11	1400	0.53			2600	0.96
B3						0.5	0.2	0.02		54	6900	2.5			12,000	4.5

Detail information on time of eruptions and SO_2 emission rates as follows: The 1979 eruption series started in June 13, 1979, and continued until December 1979 (Kyoto Univ 1980), accompanied by intense SO_2 emission (12 kg s^{-1} in September and 30 kg s^{-1} in November; Kyushu Univ 1980). The 1989 eruption started in June and continued until February 1991 (Kyoto Univ 1992; Ikebe et al. 2008), and the emission rate of SO_2 was more than 12 kg s^{-1} during most of that period (Kyushu Univ 1990, 2004). In the periods from December 1992 to February 1993 and from July 2003 to January 2004, a large SO_2 emission rate of more than 12 kg s^{-1} was observed (Kyushu Univ 2004)

[a] Chemical composition of the volcanic gas emitted from Nakadake crater on January 12, 2015, from GSJ (2015a)

[b] Water and sulfur content of degassed magma (0.12 wt% H_2O and 0.004 wt% S) was calculated from average water content of the groundmass glass (0.2 wt%) and average sulfur content of the groundmass bulk (0.006 wt%) in the 2014 scoria (Table 4) and content of groundmass in the scoria (60 wt%)

[c] The average and one standard deviation (in parenthesis) of emission rate of sulfur was calculated from averaged SO_2 flux of 157 observations in January 2014–December 2017 (1500 ± 1250 t d^{-1} SO_2; JMA 2018b), assuming that all sulfur in volcanic gas is SO_2

[d] Mass of the degassed magma was calculated for the periods from January 2014 to December 2017. The volume (m^3 DRE) was calculated from the mass, assuming a rock density of 2700 kg m^{-3}

[e] Mass of tephra in 2014–2016 was calculated from mass of tephra from November 25, 2014, to May 11, 2015 (2.1×10^9 kg; Kumamoto Univ 2015a), that of tephra on September 14, 2015, eruption (4×107 kg; Kumamoto Univ 2015b) and that of October 8, 2016, eruption (6.3×10^8 kg; Kumamoto Univ et al. 2016). The volume was calculated using a rock density of 2700 kg m^{-3}. Assuming all component of the tephra is essential, mass and volume of the tephra are equal to maximum estimates of the erupted magma

[f] Volume of the degassed magma in 1979–2017 was calculated from the $0.09–0.37 \times 10^9$ m^3 DRE the periods from June to December in 1979, $0.27–1.1 \times 10^9$ m^3 DRE from June 1989 to February 1991, $0.27–1.1 \times 10^9$ m^3 DRE from December 1992 to February 1993, $0.09–0.37 \times 10^9$ m^3 DRE from July 2003 to January and $0.62–2.5 \times 10^9$ m^3 DRE from January 2014 to December 2017. The volume of the degassed magma from June to December 1979 is more than 20 times larger than that of total tephra produced by the 1979 eruptions (0.0035×10^9 m^3 DRE; Kyoto Univ 1980; Ono and Watanabe 1985)

and B1 magmas deviated slightly toward lower K_2O contents, while those for A3 and B3 magmas were consistent with the observations (Fig. 5). This calculation suggests that a possible cause of the variations in the major-element composition of the inclusions is differences in bulk H_2O content; i.e., the inclusions with SiO_2 contents of 57–58 wt% were entrapped in magma with a bulk H_2O content of 1 wt% (A1 and B1 magmas) and the inclusions with an SiO_2 content of 59 wt% were entrapped in magma with a bulk H_2O content of 0.5 wt% (A3 and B3 magmas). This means that the magma is not homogeneous with regard to bulk H_2O content throughout the plumbing system. This inhomogeneity could be caused by a magma degassing processes such as magma convection in a conduit (e.g., Shinohara et al. 2002; Shinohara 2008).

The density contrast between magma and crust can control the ascent of magma, causing the magma to be trapped in a magma chamber if the density contrast becomes negligible (e.g., Walker 1989). The bulk density of magma is highly dependent on volatile content and bubble content. With the assumption that gas bubbles that formed from the exsolution of H_2O and CO_2 from the melt do not separate from the magma during its ascent, we calculated bulk densities of the magmas at different depths using the bulk H_2O and CO_2 contents of the magma (Table 5; Fig. 7; Additional file 3: Table S2 and Additional file 4: Table S3; Saito et al. 2005). Comparison between the bulk densities of the A1, B1, A3, and B3 magmas and that of the crust at different depths indicated that the magmas had lower bulk densities than the crust at pressures of 50–200 MPa (1–6 km depth (bsl); Table 5; Additional file 3: Table S2; Fig. 7), which would allow the magmas to ascend by buoyancy. After the magmas had ascended to 0 km depth (bsl; pressure of 25 MPa), two magma ascent processes were possible, depending on the bulk volatile content of the magma. One possibility is that the B1 magma, whose bulk density was less than that of the crust (2007 kg m^{-3} for B1 magma versus 2200–2400 kg m^{-3} for the crust at depths of < 1 km (bsl)), ascended to the surface by buoyancy and thereby caused an eruption. The other possibility is that the A1, A3, and B3 magmas, having relatively low volatile contents, encountered a density barrier at 0 km depth (bsl) because their bulk density (2400–2594 kg m^{-3}) became higher than or similar to that of the crust (Fig. 7), making it difficult for these magmas to reach the surface.

Degassed magma volume

By combining melt inclusion analysis with observations of volcanic gas, we can estimate the degassed magma volume (e.g., Kazahaya et al. 2002). We calculated the mass of degassed magma based on the estimated bulk volatile content of the magma, the measured SO_2 flux, and the chemical composition of the magmatic gas emitted from the Nakadake crater, using the following equation:

$$MV = (CM - CD) \times MD, \quad (1)$$

where MD is the mass of the degassed magma (kg), CM is the volatile content of the magma (kg kg^{-1}), CD is the volatile content of the degassed magma (kg kg^{-1}), and MV is the mass of the volatile material emitted from the crater (kg). We used the sulfur contents of A1, A3, B1, and B3 magmas (0.02–0.07 wt% S, Table 6) as the CM, because the MELTS calculation in the previous section indicated that the A1, A3, B1, and B3 magmas, with bulk H_2O contents of 0.5–1 wt%, were more realistic. The sulfur content of the degassed magma (CD) was estimated from the sulfur content of the groundmass of the 2014 scoria (Table 4), assuming that groundmass content of the scoria was 60 wt%. We calculated the amount of magma degassed over a period from January 2014 to December 2017, because of intense volcanic gas emissions combined with intermittent eruptions during that period. An average sulfur emission rate of 8.7 kg s^{-1} was calculated from the SO_2 flux observations over 157 days (1500 ± 1200 t d^{-1} SO_2; Table 6; JMA 2018b), assuming that SO_2 was the only sulfur species in the volcanic gas.

The degassing rate of the magmas over the 4-year period from 2014 to 2017 ranged from 13×10^3 kg s^{-1} to 54×10^3 kg s^{-1} (Table 6). The degassing rate of the A1 magma (13×10^3 kg s^{-1}) was similar to that of basalt–andesite volcanoes ($7–16 \times 10^3$ kg s^{-1} for Etna, Izu-Oshima, Sakurajima, and Asama volcanoes; Kazahaya and Shinohara 1996; Ohwada et al. 2013). However, the degassing rates of the A3, B1, and B3 magmas are higher than those of basalt–andesite volcanoes. The higher estimated degassing rates at Aso volcano could be caused by (1) underestimation of bulk sulfur content of the magma and/or overestimation of SO_2 flux or (2) more effective degassing and gas separation from magma at Nakadake volcano compared with the other volcanoes. More detailed studies on volcanic gas and melt inclusions will be required to evaluate these possibilities.

The volume of degassed magma estimated for 2014–2017 ($0.62–2.5 \times 10^9$ m^3 DRE) is more than 600 times larger than that of tephra over the same period (0.0010×10^9 m^3 DRE; Table 6), which is equal to the maximum estimate of erupted magma. If the lower limit for the emission rate of sulfur of 1.5 kg s^{-1} (= average of 8.7 kg s^{-1}—standard deviation of 7.2 kg s^{-1}) is used for the above calculation, the volume of the degassing magmas from 2014 to 2017 is $0.12–0.51 \times 10^9$ m^3 DRE. Even this minimum estimate is more than 100 times larger than the maximum volume of erupted magma. A

degassed magma volume so much larger than the tephra volume indicates that the volcanic gas was derived from non-erupted magma located in a deeper part of the system. Because the magma chamber is located at a depth of more than 2 km (bsl) (e.g., Sudo and Kong 2001; Hata et al. 2016), the extensive degassing could be due to magma convection in a conduit (e.g., Kazahaya and Shinohara 1996; Shinohara et al. 2002; Kazahaya et al. 2002; Shinohara 2008).

Applying the degassing rate from the 2014 eruptions, we also performed the same calculation for the periods from June 1989 to February 1991, from December 1992 to February 1993, and from July 2003 to January 2004, when a large SO_2 emission rate of more than 12 kg s^{-1} (1000 t d^{-1}) was observed (Kyushu Univ 2004). The total combined volume of degassed magma for the above periods was $1.1–4.5 \times 10^9$ m^3 DRE for the A1, A3, B1, and B3 magmas (Table 6). These estimates represent a lower limit, because the above calculation did not incorporate the emission of SO_2 during the quiescent degassing period since 1979. This estimated volume of degassing magma requires a magma chamber with a volume of at least of 1 km^3 at that depth. Geophysical observations indicate the existence of a large magma chamber at a depth of less than 10 km. Sudo and Kong (2001) proposed that this magma chamber is spherical in shape with a radius of about 3 km, corresponding to a volume of 110×10^9 m^3. The low resistivity region (C1), which has less than 10 O m (reported by Hata et al. (2016)), seems to have a major axis of about 6 km and a minor axis of about 3 km. Assuming an ellipsoid shape, this implies a volume of 28×10^9 m^3. The large magma chamber could form an important portion of the total volcanic gases emitted from the volcano from 1979 to 2017.

Summary and conclusions

The whole-rock analyses of the scoria produced by the November 26–27, 2014, eruption indicated that they are andesite in composition and identical to those of the 1979 and 1989 eruptions (Fig. 2), suggesting that these magmas were derived from the same magma chamber. Combining melt inclusion analyses of the 1979, 1989, and 2014 scoria with MELTS calculations and volcanic gas observations, we estimated the bulk volatile content of the magmas to be 0.5–1 wt% H_2O, 0.04–0.5 wt% CO_2, and 0.02–0.07 wt% S. We also estimated the amount of magma necessary to supply the SO_2 emitted from 1979 to 2017 to be $1.1–4.5 \times 10^9$ m^3 DRE (Table 6). This suggests the existence of a deep-seated andesite magma chamber with a volume larger than a few km^3. We speculate that this andesite magma chamber is the same as the one at a depth of 4–6 km (bsl), proposed by tomographic results for P- and S-wave velocity structure (Sudo and Kong 2001) and three-dimensional electrical resistivity structure (Hata et al. 2016; Fig. 7). Considering the similarity of the whole-rock composition between the 1929–1974 eruptions and the 1979–2014 eruptions (Fig. 2), this magma chamber might have existed since at least 1929.

Comparison of the densities of the andesite magma and the crust at different depths (Fig. 7) suggests that prior to each eruption in 1979, 1989, and 2014, the andesite magma ascended by buoyancy up to a depth of a few km. The saturation pressure of H_2O and CO_2 in the melt inclusions ranged from 18 to 118 MPa, corresponding to depths of 1–4 km under a lithostatic pressure gradient. Comparison of the pressure estimates with the depth of the magma plumbing system estimated by geophysical observations suggested that the inclusion entrapments occurred in an upper part of the magma chamber and/or a conduit. After the magmas had ascended to 0 km depth (bsl), the magmas with low volatile contents could have encountered a crustal density barrier, because the density contrast becomes small at that depth (Fig. 7). These magma heads that stayed at a shallow depth could supply heat and gas to the upper part of the system, which could have caused the precursor events like those that characterized the recent activity at Nakadake crater (drying-up of the crater lake water, mud eruptions, and intense volcanic gas emissions; e.g., Ono et al. 1995; Ikebe et al. 2008). The degassed magma at the head could descend in the conduit due to increases in its density, and non-degassed magma could ascend in its place by magma convection in the conduit (e.g., Kazahaya and Shinohara 1996; Shinohara et al. 2002; Kazahaya et al. 2002; Shinohara 2008). In addition, contact of these magmas with underground water or hydrothermal fluid beneath the Nakadake crater (Kanda et al. 2008) could have led to phreato- and phreato-magmatic eruptions that blew away the subsurface rocks overlying the magmas, allowing H_2O exsolution in the magmas due to pressure decrease. This caused further ascent of the magmas up to the surface and finally Strombolian eruptions. The estimated volume of degassed magma over the period from 2014 to 2017, based on bulk sulfur contents of melt inclusions, was more than 600 times larger than that of eruptive products during the same period. This suggests degassing of magma in the chamber due to magma convection in a conduit.

Additional files

Additional file 1: Fig. S1. Backscattered electron images of a clinopyroxene phenocryst containing an orthopyroxene inclusion in the 2014 scoria.

Additional file 2: Table S1. Chemical composition of rims of olivine, plagioclase, and clinopyroxene phenocrysts in the scoria from the 2014 eruption (wt%) and temperatures and pressures estimated by olivine–liquid and plagioclase–liquid thermometers and clinopyroxene–liquid thermobarometer (Putirka 2008).

Additional file 3: Table S2. Results of calculation of MELTS, density, and volume of bubbles of the magmas. The calculation was done for six types of magmas (A1, A2, A3, B1, B2, and B3) at temperatures of 1079 and 1021 °C.

Additional file 4: Table S3. Densities of H_2O and CO_2 gases at temperatures of 1021 and 1079 °C calculated by modified Redlich–Kwong equation of state (Holloway 1981).

Abbreviations

BSE: backscattered electron; bsl: below sea level; CD: volatile content of the degassed magma; CM: volatile content of the magma; DRE: dense rock equivalent; EPMA: electron probe microanalyzer; MD: mass of degassed magma; MV: mass of volatile material emitted from the crater; SEM: scanning electron microscopy; SIMS: secondary ion mass spectrometry; XRF: X-ray fluorescence analysis.

Authors' contributions

GS carried out the SEM, EPMA, and SIMS analyses of the eruptive products and the melts calculation and drafted the manuscript. OI carried out the whole-rock analyses of the eruptive products. YI performed the geological survey of the 2014 eruption at Nakadake, Aso volcano, and collected the samples. HH performed the geological survey of the 1989 and 2014 eruptions at Nakadake, Aso volcano, and collected the samples. IM participated in the SIMS analyses and performed the preliminary melts calculation. All authors read and approved the final manuscript.

Acknowledgements

We thank Drs. Maki Hata and Nobuo Matsushima for providing information on the electrical resistivity structure beneath the Aso volcano. This manuscript was greatly improved with critical and constructive comments from Drs. Corrado Cigolini and Katsuya Kaneko. This work was partly supported by Japan Society for the Promotion of Science (JSPS) KAKENHI Grant Number JP15K05274. We would like to thank Editage (www.editage.jp) for English language editing.

Competing interests

The authors declare that they have no competing interests.

Consent for publication

Not applicable.

Ethics approval and consent to participate

Not applicable.

Publisher's Note

Springer Nature remains neutral with regard to jurisdictional claims in published maps and institutional affiliations.

Received: 21 March 2018 Accepted: 5 December 2018
Published online: 14 December 2018

References

Abe Y, Ohkura T, Shibutani T, Hirahara K, Kato M (2010) Crustal structure beneath Aso Caldera, Southwest Japan, as derived from receiver function analysis. J Volcanol Geotherm Res 195:1–12. https://doi.org/10.1016/j.jvolgeores.2010.05.011

Aiuppa AC, Federico G, Giudice G, Gurrieri S (2005) Chemical mapping of a fumarole field: La Fossa Crater, Vulcano Island (Aeolian Islands, Italy). Geophys Res Lett 32:L13309. https://doi.org/10.1029/2005GL023207

Anderson AT (1973) The before-eruption water content of some high-alumina magmas. Bull Volcanol 37:530–552

Anderson AT, Newman S, Williams SN, Druitt TH, Skirius C, Stolper E (1989) H_2O, CO_2, Cl, and gas in Plinian and ash-flow Bishop rhyolite. Geology 17:221–225

Aso Volcao Museum, Kunamoto Univ, Geological Survey of Japan (1991) Recent activity and ejecta of the 1st crater of Nakadake, Aso volcano. Rep Coord Comm Predict Volcan Erupt 49:43–45 **(in Japanese)**

Asosan Weather Station (1980) Volcanic activity of Aso volcano in 1979. Rep Coord Comm Predict Volcan Erupt 17:11–29 **(in Japanese)**

Geological Survey of Japan (2015a) Variation in chemical composition of volcanic gases from Nakadake, Aso volcano. In: Paper presented at No. 131 meeting of coordinating committee for prediction of volcanic eruption, 24 February 2015 (**in Japanese**)

Geological Survey of Japan (2015b) Petrologic characteristics and volatile content of magma erupted on 26–27 November 2014 at Nakadake, Aso volcano. In: Paper presented at No. 131 meeting of coordinating committee for prediction of volcanic eruption, 24 February 2015 (**in Japanese**)

Geological Survey of Japan, Kumamoto Univ (1990) Activity and ejecta of 1989 eruptions at Nakadake 1st crater, Aso volcano. Rep Coord Comm Predict Volcan Erupt 46:59–64 **(in Japanese)**

Geological Survey of Japan, Kumamoto Univ, Aso Volcano Museum (2004) Morphology and chemical compositions of volcanic glasses in July 10, 2003 ash of Nakadake, Aso volcano, SW Japan. Rep Coord Comm Predict Volcan Erupt 86:112–117 **(in Japanese)**

Ghiorso MS, Gualda GAR (2015) An H_2O–CO_2 mixed fluid saturation model compatible with rhyolite-MEITS. Contrib Miner Petrol 169(6):53. https://doi.org/10.1007/s00410-015-1141-8

Ghiorso MS, Sack RO (1995) Chemical mass transfer in magmatic processes IV. A revised and internally consistent thermodynamic model for the interpolation and extrapolation of liquid-solid equilibria in magmatic systems at elevated temperatures and pressures. Contrib Miner Petrol 119:197–212

Gualda GAR, Ghiorso MS, Lemons RV, Carley TL (2012) Rhyolite-MELTS: a modified calibration of MELTS optimized for silica-rich, fluid-bearing magmatic systems. J Petrol 53:875–890

Hata M, Takakura S, Matsushima N, Hashimoto T, Utsugi M (2016) Crustal magma pathway beneath Aso caldera inferred from three-dimensional electrical resistivity structure. Geophys Res Lett 43:10720–10727. https://doi.org/10.1002/2016GL070315

Hauri E, Wang J, Dixon JE, King PL, Mandeville C, Newman S (2002) SIMS analysis of volatiles in silicate glasses 1. Calibration, matrix effects and comparisons with FTIR. Chem Geol 183:99–114

Holloway JR (1981) Volatile interactions in magmas. In: Newton RC, Navrotsky A, Woods BJ (eds) Thermodynamics of minerals and melts. Advances in physical geochemistry, vol 1. Springer, Berlin, pp 273–293

Ikebe S, Watanebe K, Miyabuchi Y (2008) The Sequence and Style of the Eruptions of Nakadake Aso Volcano, Kyushu, Japan. Bull Volcanol Soc Jpn 53:15–33 **(in Japanese with English abstract)**

Japan Meteorological Agency (1990) Volcanic Activity of Asosan Volcano. Rep Coord Comm Predict Volcan Erupt 47:61–70 **(in Japanese)**

Japan Meteorological Agency (2013) National catalogue of the active volcanoes in Japan (the fourth edition). Japan Meteorological Agency, Tokyo, pp 1189–1227 **in Japanese with English abstract**

Japan Meteorological Agency (2015) Volcanic activity of Asosan volcano October 2014–February 2015. Rep Coord Comm Predict Volcan Erupt 120:166–186 **(in Japanese)**

Japan Meteorological Agency (2018a) Volcanic activity of Asosan Volcano September 2017 –January 2018. In: Paper presented at No. 140 meeting of coordinating committee for prediction of volcanic eruption, 14 February 2018 (**in Japanese**)

Japan Meteorological Agency (2018b) Results of volcanic gas observation at Aso volcano. http://www.data.jma.go.jp/svd/vois/data/fukuoka/rovdm/Asosan_rovdm/Asosan_rovdm.html. Accepted 27 Feb 2018

Johnson MC, Anderson AT, Rutherford MJ (1994) Pre-eruptive volatile contents of magmas. In: Carroll MR, Holloway JR (eds) Volatiles in magmas, reviews

in mineralogy, vol 30. Mineralogical Society of America, Washington DC, pp 281–330
Kanda W, Tanaka Y, Utsugi M, Takakura S, Hashimoto T, Inoue H (2008) A preparation zone for volcanic explosions beneath Naka-dake crater, Aso volcano, as inferred from magnetoelluric surveys. J Volcanol Geotherm R 178:32–45. https://doi.org/10.1016/j.jvolgeores.2008.01.022
Kazahaya K, Shinohara H (1996) Excess degassing of active volcanoes: processes and mechanisms. Mem Geol Soc Jpn 46:91–104
Kazahaya K, Shinohara H, Saito G (2002) Degassing process of Satsuma-Iwojima volcano, Japan: supply of volatile components from a deep magma chamber. Earth Planets Space 54:327–335. https://doi.org/10.1186/BF03353031
Kilinc A, Carmichael ISE, Rivers ML, Sack RO (1983) The ferric-ferrous ratio of natural silicate liquids equilibrated in air. Contrib Miner Petrol 83:136–140
Kita TN, Ikeda Y, Togashi S, Liu Y, Morishita Y, Weisberg MK (2004) Origin of ureilites inferred from a SIMS oxygen isotopic and trace element study of clasts in the Dar al Gani 319 polymict ureilite. Geochim Cosmochim Acta 68:4213–4235
Komazawa M (1995) Gravimetric analysis of Aso volcano and its interpretation. J Geod Soc Jpn 41:17–45
Kumamoto Univ (2015a) Total mass of tephra of the eruptions at Nakadake, Aso volcano, from November 2014 to May 2015. In: Paper presented at No. 132 meeting of coordinating committee for prediction of volcanic eruption, 15 June 2015 (**in Japanese**)
Kumamoto Univ (2015b) Total mass of tephra of the eruptions at Nakadake, Aso volcano, on 14 September 2015. In: Paper presented at No. 133 meeting of coordinating committee for prediction of volcanic eruption, 21 October 2015 (**in Japanese**)
Kumamoto Univ, Geological Survey of Japan, National Res Inst for Earth Science and Disaster Prevention, Rissho Univ, Kyoto Univ, Japan Meteorological Agency (2016) Total mass of tephra of the eruptions at Nakadake, Aso volcano, on 8 October 2016. In: Paper presented at No. 137 meeting of coordinating committee for prediction of volcanic eruption, 14 February 2017 (**in Japanese**)
Kyoto Univ (1980) Review of volcanic activity of Aso volcano since 1974. Rep Coord Comm Predict Volcan Erupt 19:54 **(in Japanese)**
Kyoto Univ (1992) Recent volcanic activity of Aso volcano (October 1991–May 1992). Rep Coord Comm Predict Volcan Erupt 53:24–29 **(in Japanese)**
Kyushu Univ (1980) Observations of hot-springs and volcanic gas from Aso volcano. Rep Coord Comm Predict Volcan Erupt 17:26–29 **(in Japanese)**
Kyushu Univ (1990) Transition of SO_2 emission and density of spring CO_2 in Aso volcano (1984.1–1990.2). Rep Coord Comm Predict Volcan Erupt 46:63–68 **(in Japanese)**
Kyushu Univ (2004) Geochemical observation at Aso volcano (-January 2004). Rep Coord Comm Predict Volcan Erupt 87:83–87 **(in Japanese)**
Lowenstern JB (2003) Melt inclusions come of age: volatiles, volcanoes, and Sorby's legacy. In: De Vivo B, Bodnar RJ (eds) Melt inclusions in volcanic systems, methods, applications and problems. Elsevier, Amsterdam, pp 1–22
Machida H, Arai F (2003) Atlas of tephra in and around Japan. University of Tokyo Press, Tokyo **(in Japanese)**
Metrich N, Wallace P (2008) Volatile abundances in basaltic magmas and their degassing paths tracked by melt inclusions. In: Pukita KD, Tepley FJ III (eds) Reviews in mineralogy & geochemistry, minerals, inclusions and volcanic processes, vol 69. Mineralogical Society of America, Washington DC, pp 363–402
Metrich N, Bertagnini A, Di Muro A (2010) Conditions of magma storage, degassing and ascent at Strombori: new insights into the volcano plumbing system with inferences on the eruptive dynamics. J Petrol 51:603–626. https://doi.org/10.1093/petrology/egp083
Miyabuchi Y (2009) A 90,000-year tephrostratigraphic framework of Aso Volcano, Japan. Sediment Geol 220:169–189. https://doi.org/10.1016/j.sedgeo.2009.04.018
Miyabuchi Y (2011) Post-caldera explosive activity inferred from improved 67–30 ka tephrostratigraphy at Aso Volcano, Japan. J Volcanol Geotherm Res 205:94–113. https://doi.org/10.1016/j.jvolgeores.2011.05.004
Miyabuchi Y, Hoshizumi H, Watanabe K (2004) Late-Pleistocene tephrostratigraphy of Aso Volcano, Southwestern Japan, after deposition of AT ash. Bull Volcanol Soc Jpn 49:51–64 **(in Japanese with English abstract)**
National Research Institute for Earth Science and Disaster Prevention, Kyoto Univ, Tokyo Univ (2015a) Whole-rock chemical composition of essential products collected in the period from December 2014 to January 2015 at Nakadake crater, Aso volcano. Rep Coord Comm Predict Volcan Erupt 120:189–190 **(in Japanese)**
National Research Institute for Earth Science and Disaster Prevention, Kyoto Univ, Tokyo Univ (2015b) Whole-rock chemical composition of essential products collected on March 27, 2015 at Nakadake crater, Aso volcano. Rep Coord Comm Predict Volcan Erupt 121:248–249 **(in Japanese)**
Ohwada M, Kazahaya K, Mori T, Kazahaya R, Hirabayashi J, Miyashita M, Onizawa S, Mori T (2013) Sulfur dioxide emissions related to volcanic activity at Asama volcano, Japan. Bull Volcanol 75:775. https://doi.org/10.1007/s00445-013-0775-5
Ono K, Watanabe K (1985) Geological map of Aso volcano. Geological Map of Volcanoes, no. 4, Geological Survey of Japan, AIST (**in Japanese with English abstract**)
Ono K, Watanabe K, Hoshizumi H, Takada H, Ikebe S (1995) Ash eruption of Nakadake volcano, Aso caldera, and its products. Bull Volcanol Soc Jpn 40:133–151 **(in Japanese with English abstract)**
Papale P (2005) Determination of total H_2O and CO_2 budgets in evolving magmas from melt inclusion data. J Geophys Res 110:B03208. https://doi.org/10.1029/2004JB003033
Papale P, Moretti R, Barbato D (2006) The compositional dependence of the saturation surface of $H_2O + CO_2$ fluids in silicate melts. Chem Geol 229:78–95
Putirka KD (2008) Thermometers and barometers for volcanic systems. In: Pukita KD, Tepley FJ III (eds) Reviews in mineralogy & geochemistry, minerals, inclusions and volcanic processes, vol 69. Mineralogical Society of America, Washington DC, pp 61–120
Saito G (2005) Behavoir of volatile components in magma and magma scent and eruption processes based on melt inclusion analyses. Bull Volcanol Soc Jpn 50:S177–S192 **(in Japanese with English abstract)**
Saito G, Kazahaya K, Shinohara H, Stimac J, Kawanabe Y (2001) Variation of volatile concentration in a magma system of Satsuma-Iwojima volcano deduced from melt inclusion analyses. J Volcanol Geotherm Res 108:11–31
Saito G, Stimac JA, Kawanabe Y, Goff F (2002) Mafic-felsic interaction at Satsuma-Iwojima volcano, Japan: evidence from mafic inclusions in rhyolites. Earth Planets Space 54:303–325. https://doi.org/10.1186/BF03353030
Saito G, Uto K, Kazahaya K, Shinohara H, Kawanabe Y, Satoh H (2005) Petrological characteristics and volatile content of magma from the 2000 eruption of Miyakejima volcano, Japan. Bull Volcanol 67:268–280. https://doi.org/10.1007/s00445-004-0409-z
Saito G, Morishita Y, Shinohara H (2010) Magma plumbing system of the 2000 eruption of Miyakejima volcano, Japan, deduced from volatile and major component contents of olivine-hosted melt inclusions. J Geophys Res 115:B11202. https://doi.org/10.1029/2010JB007433
Shinohara H (2008) Excess degassing from volcanoes and its role on eruptive and intrusive activity. Rev Geophys 46:RG4005. https://doi.org/10.1029/2007rg000244
Shinohara H (2013) Composition of volcanic gases emitted during repeating Vulcanian eruption stage of Shinmoedake, Kirishima volcano, Japan. Earth Planets Space 65:667–675. https://doi.org/10.5047/eps.2012.11.001
Shinohara H, Kazahaya K, Saito G, Matsushima N, Kawanabe Y (2002) Degassing activity from Iwodake rhyolitic cone, satsuma-Iwojima volcano, Japan: formation of a new degassing vent, 1990–1999. Earth Planets Space 54:175–185. https://doi.org/10.1186/BF03353017
Shinohara H, Yokoo A, Kazahaya R (2018) Variation of volcanic gas composition during the eruptive period on 2014–2015 at Nakadake crater, Asdo volcano, Japan. Earth Planets Space 70:151. https://doi.org/10.1186/s40623-018-0919-0
Sudo Y, Kong LSL (2001) Three-dimensional seismic velocity structure beneath Aso Volcano, Kyushu, Japan. Bull Volcanol 63:326–344. https://doi.org/10.1007/s004450100145
Tamura T, Hasenaka T, Wallace P, Yasuda A, Mori Y (2015) Magma generation processes beneath volcanic front of Kyushu arc, Japan—approach from melt inclusion. Gekkan Chikyu 37:106–112 **(in Japanese)**

Togashi S (1989) XRF analytical report 1/89. Determination of major elements in igneous rocks using Sc/Mo dual anode tube. Open File Rep Geol Surv Jpn 132:1–35

Tsutsui T, Sudo Y (2004) Seismic reflectors beneath the central cones of Aso Volcano, Kyushu, Japan. J Volcanol Geotherm Res 131:33–58. https://doi.org/10.1016/S0377-0273(03)00315-9

Walker GPL (1989) Gravitational (density) controls on volcanism, magma chambers and intrusions. Aus J Earth Sci 36:149–165

Wallace PJ, Carmichael ISE (1994) S speciation in submarine basaltic glasses as determined by measurements of SKa X-ray wavelength shifts. Am Mineral 79:161–167

Yamamoto M, Kawakatsu H, Kaneshima S, Mori T, Tsutsui T, Sudo Y, Morita Y (1999) Detection of a crack-like conduit beneath the active crater at Aso Volcano, Japan. Geophys Res Lett 26:3677–3680